Water Resources Research

RESEARCH ARTICLE
10.1029/2021WR030046

The Compensatory CO_2 Fertilization and Stomatal Closure Effects on Runoff Projection From 2016–2099 in the Western United States

Xue-Yan Zhang[1], Jiming Jin[2], Xubin Zeng[1], Charles P. Hawkins[2,3], Antônio A. M. Neto[1], and Guo-Yue Niu[1]

[1]Department of Hydrology and Atmospheric Sciences, The University of Arizona, Tucson, AZ, USA, [2]Department of Watershed Sciences, Utah State University, Logan, UT, USA, [3]The Ecology Center and National Aquatic Monitoring Center, Utah State University, Logan, UT, USA

Key Points:

- Annual runoff of the major western US rivers is projected to decline variably from −11% to −92% by 2099 under Representative Concentration Pathway 8.5
- The counteracting CO_2 fertilization and stomatal closure effects on runoff are roughly compensatory
- Due to the two offsetting CO_2 effects, warming remains the dominant driver for the projected runoff decline at river basin scales

Supporting Information:

Supporting Information may be found in the online version of this article.

Correspondence to:

G.-Y. Niu,
niug@email.arizona.edu

Citation:

Zhang, X.-Y., Jin, J., Zeng, X., Hawkins, C. P., Neto, A. A. M., & Niu, G.-Y. (2022). The compensatory CO_2 fertilization and stomatal closure effects on runoff projection from 2016–2099 in the western United States. *Water Resources Research*, *58*, e2021WR030046. https://doi.org/10.1029/2021WR030046

Received 24 MAR 2021
Accepted 22 DEC 2021

Author Contributions:

Conceptualization: Xue-Yan Zhang, Jiming Jin, Guo-Yue Niu
Data curation: Xue-Yan Zhang
Formal analysis: Xue-Yan Zhang, Guo-Yue Niu
Funding acquisition: Jiming Jin, Xubin Zeng, Charles P. Hawkins, Guo-Yue Niu
Investigation: Xue-Yan Zhang
Methodology: Xue-Yan Zhang, Guo-Yue Niu
Resources: Xue-Yan Zhang, Guo-Yue Niu
Software: Xue-Yan Zhang
Supervision: Jiming Jin, Guo-Yue Niu
Validation: Xue-Yan Zhang
Visualization: Xue-Yan Zhang
Writing – original draft: Xue-Yan Zhang, Guo-Yue Niu

Abstract Water availability in the dry western United States (US) under climate change and increasing water use demand has become a serious concern. Previous studies have projected future runoff changes across the western US but ignored the impacts of ecosystem response to elevated CO_2 concentration. Here, we aim to understand the impacts of elevated CO_2 on future runoff changes through ecosystem responses to both rising CO_2 and associated warming using the Noah-MP model with representations of vegetation dynamics and plant hydraulics. We first validated Noah-MP against observed runoff, leaf area index (LAI), and terrestrial water storage anomaly from 1980 to 2015. We then projected future runoff with Noah-MP under downscaled climates from three climate models under Representative Concentration Pathway 8.5. The projected runoff declines variably from the Pacific Northwest by −11% to the Lower Colorado River basin by −92% from 2016 to 2099. To discern the exact causes, we conducted an attribution analysis of the modeled evapotranspiration from two additional sensitivity experiments: one with constant CO_2 and another one with static monthly LAI climatology. Results show that surface "greening" (due to the CO_2 fertilization effect) and the stomatal closure effect are the second largest contributors to future runoff change, following the warming effect. These two counteracting CO_2 effects are roughly compensatory, leaving the warming effect to remain the dominant contributor to the projected runoff declines at large river basin scales. This study suggests that both surface "greening" and stomatal closure effects are important factors and should be considered together in water resource projections.

Plain Language Summary Water shortage in the western United States (US) is becoming increasingly serious due to increasing socioeconomic demands and climate change. Although previous studies have projected various degrees of runoff changes, they neglect the impact of rising CO_2 on runoff projections. To explore the possible role that CO_2 may play in the hydrologic cycle, we conducted three experiments with the newly improved Noah-MP land model including vegetation dynamics and plant hydraulics. Consistent with previous studies, the western US tends to be drier toward the end of the 21st Century. CO_2-induced leaf area index increases (surface "greening") contribute considerably to the projected widespread transpiration increases and runoff reductions; however, these changes are nearly compensated by the stomatal closure effect of CO_2 on transpiration, leaving the warming effect to remain the major cause to these transpiration and runoff changes. Therefore, the dual roles of CO_2 in the hydrologic cycle through interactions with vegetation processes need to be considered in water resource projections.

1. Introduction

Water availability in the dry western United States (US) under increasing water demands and climate change has become a serious concern. Expanding population, increasing total water use, and rapidly growing agriculture in the western US, have posed a great challenge on sustainable management of water resources (Anderson & Woosley, 2006). Besides, restoration of endangered riparian ecosystems related to depleted water resources, which has recently received an increasing attention, requires more water in the episodes of droughts (Anderson & Woosley, 2006). In addition to substantial water demands, significant reductions in annual runoff yield have been observed across the western US due to climate change (Forbes et al., 2018), with earlier snowmelt runoff and reduced summer flows (Clow, 2010; Hamlet et al., 2007). It is crucial to discern the controlling factors of runoff for reducing the uncertainties in future runoff and water resource projections.

Writing – review & editing: Xue-Yan Zhang, Jiming Jin, Xubin Zeng, Charles P. Hawkins, Antônio A. M. Neto, Guo-Yue Niu

Runoff generation is largely affected by static factors, for example, soil property and topography, and changes in climate and associated ecosystem response. Changing precipitation patterns, such as amounts as well as intensity, duration, and frequency, directly affect runoff generation. Rising temperatures can enhance evapotranspiration (ET) through increases in the atmospheric water demand and induce a greater loss of snow mass with a shrinking snow cover, causing a positive feedback to the warming (Milly & Dunne, 2020). Also, changes in other climate variables, such as downward longwave radiation, wind speed, and atmospheric humidity contribute substantially to changes in ET (McVicar et al., 2012), resulting in totally different extent of dryland expansion (Sheffield et al., 2012). Terrestrial ecosystem plays a key role in the terrestrial hydrologic cycle (Lemordant et al., 2018; Ukkola et al., 2016) through root water uptake, transpiration, canopy interception loss, and hydraulic redistribution. Recent studies, however, show conflicting effects of vegetation responses to elevated CO_2 concentration. Singh et al. (2020) suggested that increases in leaf area index (LAI) and plant water use efficiency (WUE) due to elevated CO_2 result in an insignificant trend in the observed runoff in the southeastern US during 1951–2015. Y. Yang et al. (2016) reported minor changes in LAI and leaf-level transpiration under elevated CO_2 in 18 tropical forest catchments over 1982–2010 based on in situ and satellite observations. Yet, Frank et al. (2015) found CO_2-induced increases in plant WUE cannot nullify increases in transpiration caused by increases in LAI and temperature across the European forests during the twentieth century. Ukkola et al. (2016) suggested that the projected runoff reductions caused by changing climate may be moderated (exacerbated) because of reduced (increased) vegetation growth in wet and humid (dry) Australia. Y. Yang et al. (2021) found regional differences in the CO_2-induced historical runoff changes and attributed them to differences in resource availabilities (e.g., water and energy), suggesting a larger CO_2-induced runoff reduction in low resource (semiarid and arid) regions. Although consistent temperature increases and slight precipitation changes are projected for the western US (Easterling et al., 2017; Vose et al., 2017), whether the vegetation response to elevated CO_2 and associated climate change alleviate or aggravate the future water shortage over the already dry western US remains very uncertain.

Raw runoff outputs from Earth system models (ESMs) are not generally used in regional hydrologic projections. The coarse horizontal resolution of ESMs (~100 km) poorly characterizes the heterogeneity in the soil, vegetation, and topographic characteristics. The low spatial resolution may result in uncertainties in the water balance in hydrologic projections and may miss key hydrologic processes in current ESMs, such as soil water-groundwater interactions and subsurface lateral flows (Fan et al., 2019; Sun et al., 2016). More importantly, current land surface models (LSMs) used in ESMs do not adequately represent plant drought resilience, producing an unrealistically decreasing LAI trend in most drying drylands (Mao et al., 2013). During droughts, these models produce unrealistically low rain use efficiency (biomass productivity per unit rainfall; Ma et al., 2017; Zhu et al., 2019). Inadequate representations of plant and root hydraulics, especially under a changing climate, may result in low transpiration and high runoff. Most recent models have started to implement plant hydraulics (Kennedy et al., 2019; L. Li, Rodell, et al., 2021; Niu et al., 2020; S. Zhu, Piao, et al., 2017) and explicitly represent plant water storage supplied by dynamic root water uptake and groundwater capillary rise to enhance ecosystem resilience to drought stress (Niu et al., 2020).

A number of previous studies, to project future water availability, used offline LSMs driven by downscaled ESM's atmospheric outputs of temperature and precipitation but ignored the impacts of other atmospheric variables and the vegetation response to elevated CO_2 (Hamlet & Lettenmaier, 1999; Naz et al., 2016; Sun et al., 2016). Hamlet and Lettenmaier (1999) used a "delta" method to perturb historical climate data by mapping spatially averaged future changes in precipitation and temperature resulting from global climate models (GCMs) relative to their historical records. They reported that the annual runoff of the Columbia River Basin in 2045 would be 85%–110% of that of 1961–1997. Naz et al. (2016) projected an increase in runoff in spring and winter but widespread summer runoff declines in the mid-century (2011–2050) compared to the baseline period (1966–2005) with the VIC hydrological model driven by the downscaled and high-resolution precipitation and temperature from 10 climate models of the Fifth Phase of the Coupled Model Intercomparison Project (CMIP5) under the Representative Concentration Pathway (RCP) 8.5. Sun et al. (2016) projected more than 20% annual runoff declines in the central part of the western US during 2031–2060 compared to that during 1979–2007, except in the Lower Colorado River basin (due to more projected precipitation than ET). However, these previous studies considered only the impacts of temperature and precipitation but neglected the impacts of other forcing variables including downward longwave radiation, wind speed, and specific humidity that show an apparent trend (Figure S1 in Supporting Information S1) and thus may directly affect the projected ET and runoff trends as well as dryland expansion (Sheffield et al., 2012). In addition, these offline studies neglected the significant rise of CO_2 and

related ecohydrological consequences. Ignoring the vegetation response to elevated CO_2 in these offline studies may overestimate droughts compared to direct outputs from coupled models (Milly & Dunne, 2017; Roderick et al., 2015; Y. Yang et al., 2019; Y. Yang et al., 2020).

A widespread surface "greening" over the boreal forests and drylands has been observed and attributed to the CO_2 fertilization effect under a warming climate (Fensholt et al., 2012; Z. Zhu, Piao, et al., 2017). Also, despite a drying trend (Chang et al., 2020), arid and semiarid ecosystems have been greening as evidenced from pronounced greenness increases (Fensholt et al., 2012), large-scale woody encroachment (Andela et al., 2013), and enhanced net carbon sinks (Ahlström et al., 2015) over global drylands. This is well explained by an analysis based on the gas exchange theory (Donohue et al., 2013). Z. Zeng et al. (2018) reported that vegetation greening has contributed to over 50% of global ET increases during the past three decades. However, plant stomatal closure and increased WUE caused by elevated CO_2 concentration may result in less transpiration at the leaf level scale (Field et al., 1995). The CO_2 inhibition effect on stomatal opening is widely used in interpreting runoff changes projected by ESMs with the conceptual Penman-Monteith & Budyko framework (Milly & Dunne, 2016; Y. Yang et al., 2019). Therefore, the model projected future runoff change may be largely controlled by the relative importance of these two counteracting CO_2 effects to terrestrial ecosystem responses, whereas surface "greening" induced by the CO_2 fertilization effect is greatly affected by model representations of ecosystem resilience to increasing drought stress (Niu et al., 2020).

In this study, we aim to discern the dominant processes controlling the projected future runoff changes using the Noah-MP LSM (Niu et al., 2011) with explicit representations of vegetation dynamics and plant hydraulics (Niu et al., 2020). Here, our specific objectives are to (a) project future runoff changes in the western US; (b) quantify the impacts of LAI changes (or "greening") and stomatal closure on ET changes using the Penman-Monteith (PM) equation; (c) investigate the role of the two counteracting effects of CO_2 ("greening" and stomatal closure) playing in the hydrologic cycle. We first performed future projections of runoff and factors influencing runoff generation in the western US under the RCP 8.5 scenario with Noah-MP. We then conducted an attribution analysis on the modeling results based on the PM equation (Y. Yang et al., 2019) and isolated the two counteracting CO_2 effects on the projected changes in ET and runoff through model sensitivity experiments with a constant CO_2 concentration and static leaf dynamics, respectively.

2. Materials and Methods

2.1. Data

2.1.1. Forcing, Vegetation, and Soil Data

We used the Phase 2 of the North American Land Data Assimilation System (NLDAS-2) atmospheric forcing data (Xia et al., 2012) to drive Noah-MP during the historical period from 1980 through 2015. This dataset spans from January 1979 to present at a resolution of 0.125° with an hourly time step throughout the contiguous US (CONUS). NLDAS-2 provides hourly downward shortwave and longwave radiation fluxes, surface air pressure and temperature, specific humidity, wind speed, and precipitation rate. NDLAS-2 has been widely verified and employed in modeling studies over the CONUS domain (Ma et al., 2017; Xia et al., 2012). We used the global 1-km hybrid State Soil Geographic Database and the USGS 24-category vegetation data, which were resampled to fit the NLDAS-2 resolution to determine the dominant soil and vegetation types (for use in Noah-MP) over the western US in both the historical and future simulations.

We used the CMIP5 climate models' output (Taylor et al., 2012) for future projections. Nonlinear yearly CO_2 concentration (Prather et al., 2013) was used to represent future CO_2 changes (Figure S2 in Supporting Information S1). We selected the model outputs from three CMIP5 GCMs experiments under RCP 8.5 because they provide sub-daily atmospheric variables for driving Noah-MP, including GFDL-ESM2G (at 2.0° × 2.5°), MIROC5 (1.4° × 1.4°), and IPSL-CM5A-MR (1.3° × 2.5°). The RCP 8.5 scenario was selected, because it may magnify the signal of vegetation response given the highest CO_2 growth rate, thereby facilitating process understanding. The three models represent divergent future climate changes, where the most aggressive increase in air temperature occurs in IPSL-CM5A-MR (Buotte et al., 2019), with the least temperature increase in GFDL-ESM2G (Figure S1 in Supporting Information S1). We downscaled these 3-hourly data (except precipitation) to the resolution of NLDAS-2 through bilinear interpolation and corrected the biases of the downscaled data using linear regression models by retaining the probability distributions of historical values similar to those of NLDAS-2 (Dettinger

et al., 2004). However, this method struggles to reproduce historical patterns of the precipitation extremes. We then interpolated the daily precipitation data (Abatzoglou, 2013) from the selected GCMs to a spatial resolution of 0.125° by bilinear interpolation and disaggregated into a temporal resolution of 3 hr following the method described by Buotte et al. (2019). This method first calculates the ratio of the 3-hourly CMIP5 precipitation to the daily CMIP5 precipitation total and then disaggregated the Multivariate Adaptive Constructed Analogs daily precipitation product based on these ratios over each grid cell. Through downscaling and bias-corrections, the biases in these GCM outputs are largely reduced for the historical period (Figure S1 in Supporting Information S1).

2.1.2. Observational Data

To calibrate and evaluate the Noah-MP's performance, we used ground-based runoff, satellite-derived LAI and terrestrial water storage (TWS) change, upscaled FLUXNET data of gross primary production (GPP) and ET using model tree ensemble (FLUXNET MTE), and ground-based snow water equivalent data (SWE; Broxton et al., 2016; Dawson et al., 2017; X. Zeng et al., 2018). We calibrated and validated the simulated runoff during 1980–2015 against the USGS WaterWatch monthly runoff data at two-digital hydrological unit code, HUC2 (Seaber et al., 1987) basins (Rivers 14–18; Figure 1). This runoff dataset is generated using stream gage observations, the corresponding drainage basins, and HUC2 boundaries (Brakebill et al., 2011), which has been taken as a surrogate of natural streamflow (Ashfaq et al., 2013; Ma et al., 2017). We selected a consistent and continuous LAI product to evaluate the simulated LAI, which is an improved product (Yuan et al., 2011) of the Moderate-Resolution Imaging Spectroradiometer (MODIS) LAI at a spatial resolution of 1 km and a temporal resolution of 8 days. We upscaled this LAI dataset into the resolution of NLDAS-2 (0.125°) and aggregated it into a monthly product during 2002–2015.

Because of high uncertainties related to current ET products (Mueller et al., 2011), we indirectly evaluated ET simulations using the terrestrial water storage anomaly (TWSA) product derived from gravity changes detected by the Gravity Recovery and Climate Experiment (GRACE) twin satellites. We used three 1° monthly GRACE TWSA products together with their gain factors (to reduce leakage error) and averaged these datasets for the period of 2003–2015 (Landerer & Swenson, 2012; Sakumura et al., 2014). The FLUXNET MTE dataset is generated by upscaling water, CO_2, and energy fluxes measured at FLUXNET sites, which are densely located in the US, and incorporating remote sensing, meteorological, and land cover data through a machine learning approach (Jung et al., 2011).We downscaled 0.5° GPP and ET datasets of FLUXNET MTE to 0.125° to assess the modeled GPP and ET using a bilinear interpolation method (Ma et al., 2017). The daily SWE product is developed using in situ observations and 4-km gridded PRISM precipitation and temperature data and has been a benchmark for large-scale SWE evaluations (Broxton et al., 2016; Cho et al., 2020). We reprocessed the daily SWE data into a spatial resolution of 0.125° through the bilinear interpolation method and a monthly temporal resolution to evaluate the simulated SWE.

2.2. Model

We used Noah-MP (Niu et al., 2011), a widely used LSM that simulates the exchanges of energy, water, and carbon between the terrestrial ecosystem and the atmosphere. The model includes one canopy layer, up to three snow layers depending on snow depth, four soil layers with a total depth of 2 m, and an unconfined aquifer. Noah-MP represents surface heterogeneity with a "semi-tile" scheme that separately computes energy, water, and carbon fluxes for vegetated and bare fractions of a model grid cell (Niu et al., 2011). Surface runoff and subsurface runoff are parameterized as functions of water table depth based on the TOPMODEL concept (Niu et al., 2005).

Noah-MP adopts the simple bucket-type groundwater model of Niu et al. (2007) to represent groundwater recharge into the aquifer (or "bucket") in wet periods and groundwater capillary rise from the "bucket" during dry periods. It also introduces a scaling factor, f_{mic}, (between 0 and 1; fraction of micropore volume) to reduce the capillary rise to account for the presence of subsurface macropores and thus helps improve the modeled soil moisture variability in the State of Illinois (Z. L. Yang et al., 2011). In general, a larger f_{mic} produces a wetter soil with smaller soil moisture variabilities. In this study, we used a constant f_{mic} of 0.3 for all experiments over the western US. The hydraulic conductivity of the aquifer (K_a) is parameterized as a harmonic mean of that of the bottom soil layer (K_b) and that at the water table (K_{sat}): $K_a = 2\,K_{\text{sat}}\,K_b/(K_{\text{sat}} + K_b)$, where K_{sat} is the saturated hydraulic conductivity. Groundwater capillary rise is demonstrated important for plants to survive drought stress over the central US basins (Niu et al., 2020).

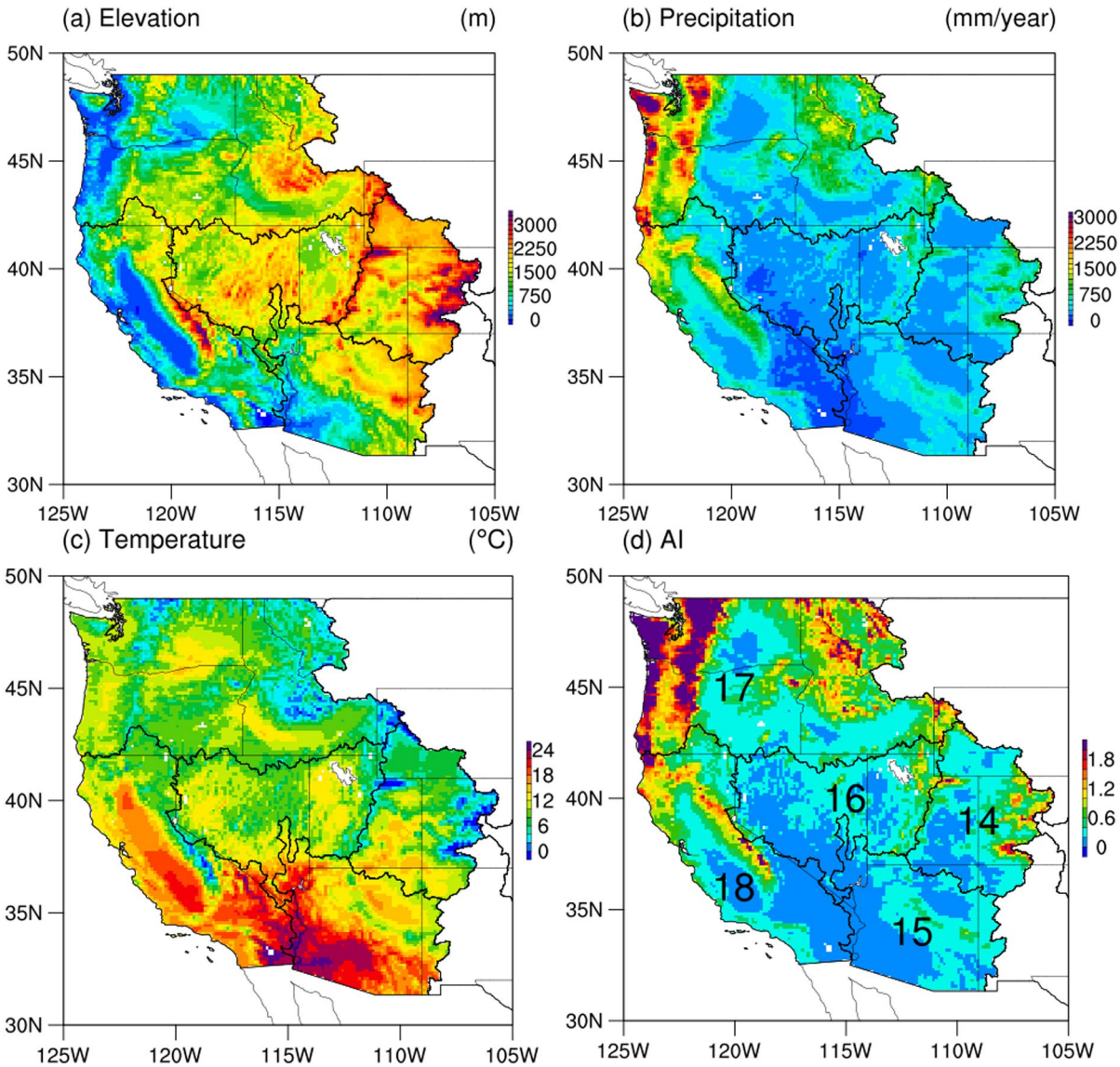

Figure 1. (a) Elevation (m), (b) mean precipitation (mm/year), (c) mean near-surface air temperature (°C), and (d) aridity index (precipitation/potential evapotranspiration) during 1980–2015. The polygons represent the boundaries of the USGS two-digital hydrologic unit code regions with their corresponding two-digit codes: 14: Upper Colorado, 15: Lower Colorado, 16: Great Basin, 17: Pacific Northwest, 18: California.

Noah-MP incorporates a simple but efficient dynamic vegetation model (Niu et al., 2011). This model explicitly represent photosynthesis, carbon allocation, respiration, turnover, and leaf death due to temperature and water stresses (Dickinson et al., 1998; Niu et al., 2011; Parton et al., 1978). Noah-MP calculates the gross photosynthesis rate, A, as a sum of leaf-level gross photosynthesis rate, A_i (μmol CO_2 m^{-2} s^{-1}; $i = 1, 2$ for sunlit and shaded leaves per unit leaf area, respectively), weighted by sunlit and shaded LAI. The leaf-level A_i is calculated as the minimum of three limiting carboxylation rates: the light-limited rate, the Rubisco-limited rate, and the limitation by the transport of photosynthate for C_3 and C_4 plants (Collatz et al., 1992; Farquhar et al., 1980). Noah-MP represents the leaf-level stomatal conductance, $g_{s,i}$ and A_i under the control of abiotic factors, such as atmospheric humidity and CO_2 concentration, c_a, for sunlit and shaded leaves (Ball et al., 1987):

$$g_{s,i} = g_0 + m\frac{A_i}{c_s}\frac{e_s}{e_i}P_{\text{atm}} \quad (1)$$

where c_s is the CO_2 concentration at the leaf surface (Pa) controlled by intermittent turbulent diffusion of c_a through the leaf boundary layer: $c_s = c_a - A_i P_{atm}/(1.37 r_b)$, where r_b is the leaf boundary layer resistance; e_s and e_i are the water vapor pressure at the leaf surface ($e_s = \frac{\frac{e_a}{g_{s,i}} + e_i r_b}{\frac{1}{g_{s,i}} + r_b}$, where e_a is the atmospheric water vapor pressure, Pa) and the saturated vapor pressure inside the leaves (Pa) at leaf surface temperature, respectively; g_0 is the minimum conductance (μmol m^{-2} s^{-2}); m is the slope constant of the $g_{s,i} - A_i$ relationship; P_{atm} is the atmospheric pressure (Pa). Because A_i for the light-limited and Rubisco-limited rates of C_3 plants and transport-limited rate of C_4 plants is linked to the intercellular CO_2 concentration, $C_i = C_a - \frac{A_i P_{atm}}{1.37 r_b + \frac{1.65}{g_{s,i}}}$, Noah-MP iteratively solves the above equation with a first guess of $c_i = 0.7\, c_a$ for C_3 plants and $c_i = 0.4\, c_a$ for C_4 plants. Because $g_{s,i}$ is inversely related to c_s [Equation 1], a higher c_s due to elevated c_a results in a reduction in $g_{s,i}$ and subsequently a reduction in leaf-level transpiration, inducing a "stomatal closure" effect on transpiration. On the other hand, A_i increases with increasing c_i controlled by the diffusion of c_a through the leaf boundary layer and plant stomata. LAI increases with increasing assimilated carbon (A_i), resulting in a "surface greening" effect on transpiration.

Reduction in A_i due to soil water stress is parameterized through the control of plant water availability, β, on the optimum carboxylation rate at 25°C. The Noah-MP version used in this study also includes a dynamic root submodule that explicitly describes plant water storage supplied by dynamic root water uptake through hydrotropic root growth to meet the transpiration demand (Niu et al., 2020). The root water uptake at a root layer is linked to root surface area density within the layer, being converted from the model-predicted root carbon mass in the layer. The latter is controlled by the photosynthate being translocated to roots, root exudates, maintenance/growth respiration, and root turnover due to temperature and water stresses. The model allows more carbon translocation to roots when the plants are under water stress and represents root hydrotropism through more carbon translocation to roots in wetter soil layers but with less turnover following Parton et al. (1978). The plant water availability factor β controlling A_i and $g_{s,i}$ is parameterized as a function of water storage in the living plant tissues, M_q (Niu et al., 2020).

$$\beta = \min\left(1.0, \frac{M_q - M_{q,\text{wilt}}}{M_{q,\max} - M_{q,\text{wilt}}}\right) \tag{2}$$

where $M_{q,\text{wilt}}$ represents the minimum plant water storage at the wilting point of 30 bar (306 m or 3.0 MPa), and $M_{q,\max}$ the maximum plant water storage when the plants are at full hydration. $M_q - M_{q,\text{wilt}}$ is the plant water available for transpiration, and ($M_{q,\max} - M_{q,\text{wilt}}$) is the maximum water that a plant can lose through transpiration until its wilting point. M_q is depleted by transpiration while supplied by root water uptake, which is further controlled by root surface area that is converted from root biomass at each layer and the water pressure gradient between the soils and the roots. Compared to the static root in previous versions of Noah-MP, the current version greatly improve plant drought resilience through hydrotropic root growth and groundwater capillary rise in the central US (Niu et al., 2020).

2.3. Model Experiments

We conducted two sets of simulations using Noah-MP with the parameterization schemes including all recent improvements (Table S1 in Supporting Information S1): a historical simulation from 1980 to 2015 using the hourly NLDAS-2 forcing and projections from 2016 to 2019 driven by the 3-hourly, downscaled climatic forcing. The historical simulation, starting with arbitrary initial states and a constant CO_2 concentration of 360 ppm, was spun up for seven times from 1980 through 2015 (mainly for TWS anomaly), and the last loop was used for analysis. The future projections were performed with the downscaled and bias-corrected forcing data from 2016 to 2099. The initial conditions for future projections were from the last loop of the historical simulation of Noah-MP driven by downscaled GCM outputs during 1980–2015.

In the set of future projections, we conducted three experiments: (a) using Noah-MP with the RCP 8.5 CO_2 concentration (hereafter CTRL); (b) based on CTRL but with the constant CO_2 of 1980 concentration (CON-CO2); and (c) based on CTRL but with the monthly LAI climatology of MODIS LAI (averaged from 2002 to 2015), which is "static" without year-to-year variations (STATIC-LAI). These three experiments are designed to discern the surface greening effect and stomatal closure effect: CTRL includes both effects; STATIC-LAI removes the

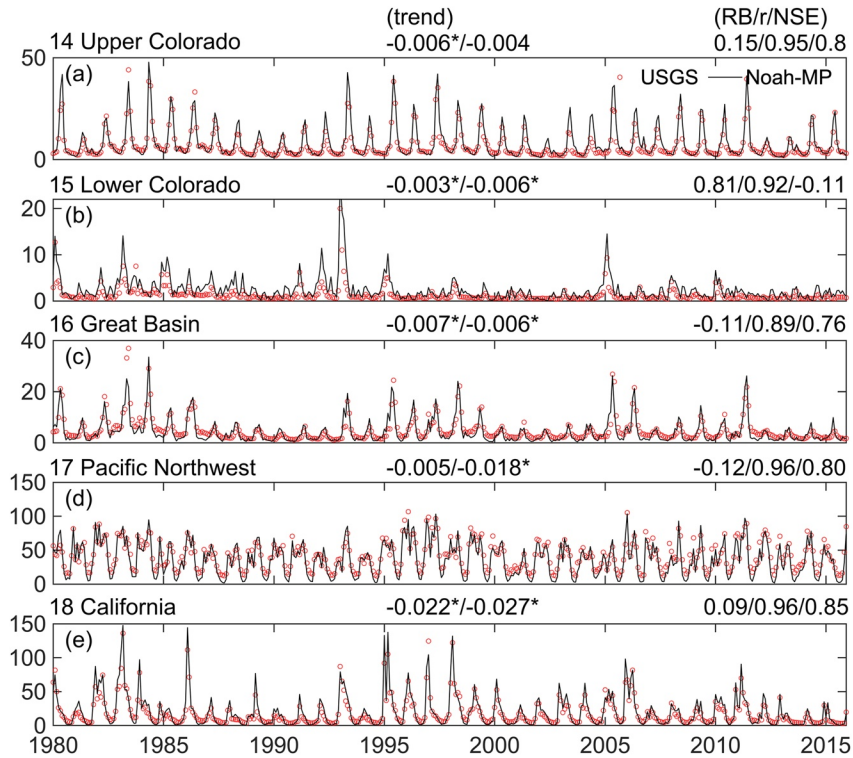

Figure 2. The Noah-MP simulated (black lines) and observed monthly runoff (red circles) during 1980–2015 of the two-digital hydrologic unit code (HUC2) river basins in the western US (unit: mm/month): (a) the Upper Colorado (River 14), (b) the Lower Colorado (River 15), (c) the Great Basin (River 16), (d) the Pacific Northwest (River 17), and (e) California (River 18). The legend provided in (a) applies to all other parts. Also shown on top of each panel are the linear trend (mm/month/month) of the observed/modeled and model evaluation metrics in the order of RB/r/NSE. The asterisks indicate that trends pass the non-parametric Mann-Kendall significance test ($p < 0.05$). RB = relative bias; r = Pearson correlation coefficient; NSE = Nash-Sutcliffe efficiency.

greening effect but retains the stomatal closure effect; and CON-CO2 excludes the stomatal closure effects and significantly reduces the LAI trends compared with those in CTRL (to be discussed later in Section 3.4).

To evaluate Noah-MP modeled runoff, LAI, TWSA, GPP, ET, and SWE, we calculated the relative bias (RB), Pearson Correlation coefficient (r), Nash-Sutcliffe efficiency (NSE), and linear trends between simulations and observations using USGS WaterWatch runoff, MODIS LAI, GRACE TWSA, FLUXNET MTE, and observed SWE datasets across the western US, respectively. For the projection results, we calculated long-term linear trends of annual runoff, LAI, transpiration, and ET during 2016–2099 and examined the significance of these trends using the nonparametric Mann-Kendall test. We also analyzed the contribution of net radiation (R_n), vapor pressure deficit (vpd), surface resistance (r_s), aerodynamic resistance (r_a), and the slope of the saturation vapor pressure–temperature relationship (δ) to the projected ET changes using the PM equation (see Appendix A). More importantly, we isolated the contribution of the surface greening and stomatal closure effects through the difference between the model experiments using the PM equation.

3. Results

3.1. Model Evaluation

The modeled runoff is comparable with the USGS WaterWatch runoff data from 1980 through 2015 over the five HUC2 rivers (Figure 2). The RB, r, and NSE values are less than 15%, above 0.89, and over 0.76 for most regions, respectively. The relatively large RB of 81% and low NSE of −0.11 for the Lower Colorado are due mainly to the overestimated NLDAS-2 precipitation (Ma et al., 2017); the NLDAS-2 precipitation cannot balance the sum of USGS runoff and FLUXNET ET estimates for a 30-year period (1982–2011). To improve the model

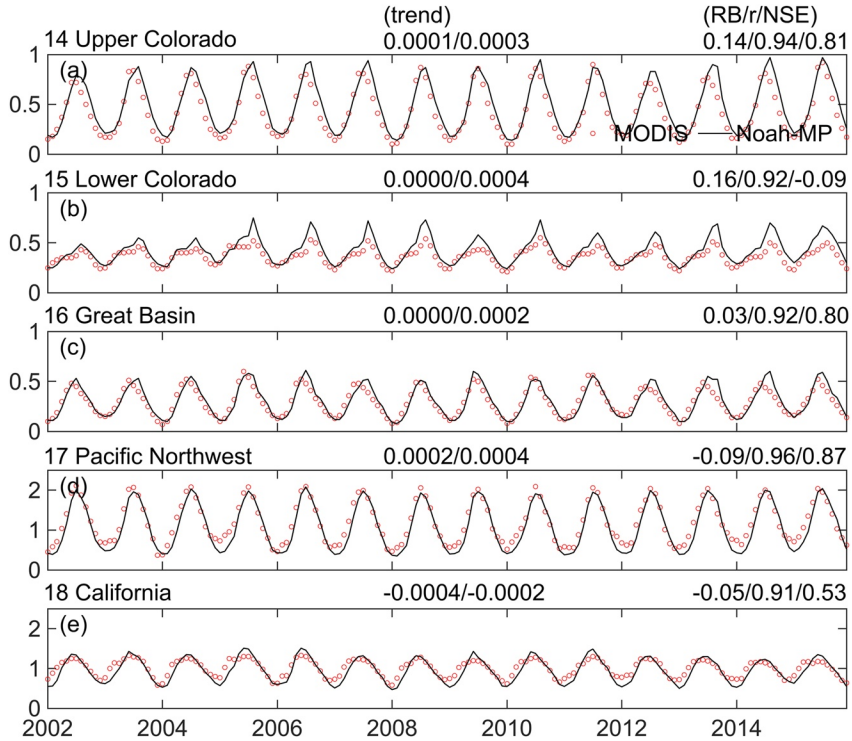

Figure 3. Same as Figure 2 but for monthly leaf area index during 2002–2015 (unit: m^2/m^2). The trend unit is m^2/m^2/month.

performance in the Lower Colorado, we need to further calibrate a spatially constant parameter, dry soil layer depth, in the surface soil resistance to enhance soil surface evaporation (Sakaguchi & Zeng, 2009; Swenson & Lawrence, 2014) and thereby reducing runoff. The value of the dry soil layer depth parameter may compensate for the deficiency in the precipitation input, which could impact the sensitivity of the simulations to future changes in climates and CO_2 levels. Noah-MP well reproduces the observed declining trends in runoff, despite slight overestimations of the observed decreases in most rivers. The simulated LAI agrees with the observed monthly LAI during 2002–2015 over most of the rivers (Figure 3) with RB values of less than 15%, r values of over 0.91, and NSE values of over 0.53, respectively, except the Lower Colorado, where Noah-MP overestimate LAI by 16%, resulting in a negative NSE (−0.09; Figure 3b) in response to the overestimated precipitation input. Both the simulated and observed LAI values do not exhibit apparent trends in all rivers, due possibly to little change in CO_2 concentration during this short period (2002–2015).

We also compared the simulated monthly TWSA with GRACE TWSA during 2003–2015 (Figure 4). The simulated monthly TWSA is derived by subtracting the monthly mean of the simulated TWS during 2004–2009 to be consistent with the procedure of the GRACE TWSA products. Here, the modeled TWS is the sum of SWE, soil moisture, groundwater storage, canopy water, and the plant water storage. The simulated TWSA agrees well with GRACE in phase and variability in most rivers, with the r and NSE values being above 0.81 and 0.29, respectively. Promisingly, Noah-MP captures well the observed TWSA trends, except in the Upper Colorado that is likely due to the uncertain climate inputs in the last two years (2014 & 2015), suggesting that the ET trend is also well simulated. Noah-MP also shows comparable estimations of ET and GPP with those of FLUXNET MTE and of SWE with those of observed SWE over each river basin, respectively (Figures S3–S5 in Supporting Information S1). Overall, the good agreement between the simulated and the observed runoff, LAI, TWSA, and relevant variables ensures an improved credibility of Noah-MP for projected future runoff and vegetation changes.

3.2. Projected Runoff Changes

The Noah-MP projected runoff declines remarkably across the western US rivers in the future under the different climate produced by the three different GCMs (Figure 5a). The annual runoff averaged over these rivers decreases by up to −71% during 2016–2099 (−12 mm/year/decade), −92% (−6 mm/year/decade), −52% (−5 mm/year/

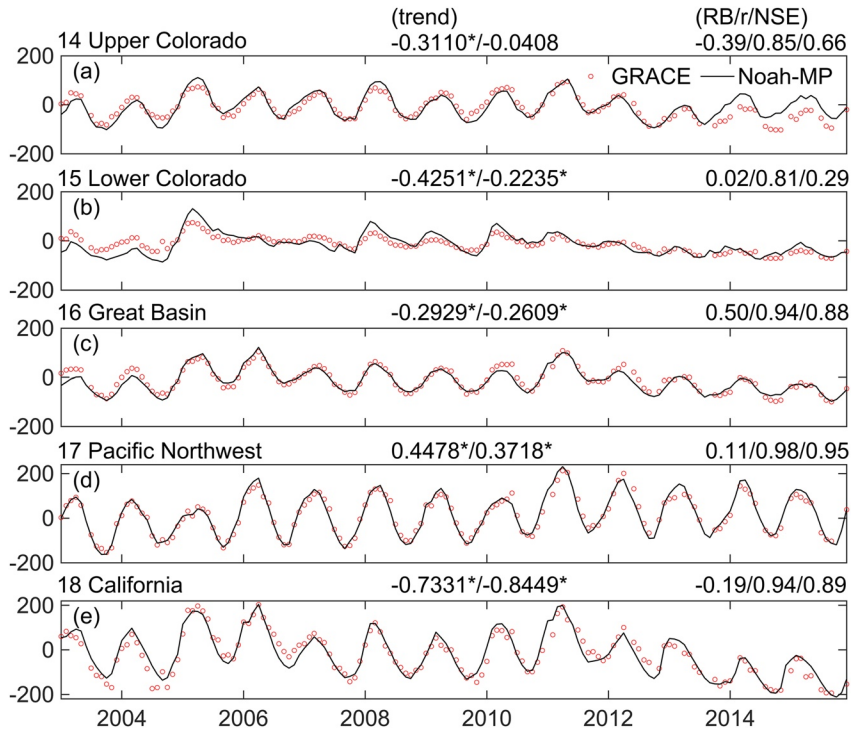

Figure 4. Same as Figure 2 but for monthly terrestrial water storage anomaly during 2003–2015 (unit: mm/month). The trend unit is mm/month/month.

decade), −11% (−7 mm/year/decade), and −30% (−13 mm/year/decade), over River 14 to River 18, respectively. The trends with a unit of percent in this study were calculated as the total linear changes relative to the linear fit of the starting year (2016). The projected TWS also exhibits substantial decreasing trends at a rate of −134, −152, −104, −2, and −49 mm/year/decade over these rivers, respectively (Figure 5c), resulting in deeper water tables because groundwater storage changes accounts for the majority of TWS reductions (see Figures 8f and 8h). Therefore, the model differences in the annual runoff trends are generally consistent with those in the modeled TWS trends. Insignificant precipitation changes ($p > 0.05$; Figure 5b) and substantial TWS declines ($p < 0.05$) indicate that ET changes likely control the future runoff trends for the western US, based on the annual water balance. Overall, the runoff reductions in the western US rivers are due mainly to increases in ET, which will be further discussed in the next section. However, the decreased annual runoff over the Lower Colorado from IPSL-CM5A-MR and MIROC5 and over the Upper Colorado from IPSL-CM5A-MR result from decreasing precipitation (Figure 5b) and from the smaller magnitudes of ET decreases (Figure 6).

3.3. Projected LAI and ET Changes

From 2016 to 2099, the projected annual mean LAI across the western US exhibits an increasing trend under all the three climates produced by different GCMs (Figure 6a). The annual LAI increases by 92% (0.06 m^2/m^2/decade), 77% (0.05 m^2/m^2/decade), 101% (0.04 m^2/m^2/decade), 60% (0.08 m^2/m^2/decade), and 57% (0.07 m^2/m^2/decade) over River 14 to River 18, respectively. We will show later that these increasing trends are mainly attributed to the rising CO_2 through comparison with the constant CO_2 experiment (see Section 3.4). Increases in the summer LAI (Figure S6 in Supporting Information S1) resulting from IPSL-CM5A-MR are less than those from GFDL-ESM2G due mainly to its relatively high temperatures over the optimum temperature (25°C) for photosynthesis in all the rivers except the relatively colder Pacific Northwest. The differences in LAI changes for other three seasons between 2016–2045 and 2070–2099 are smaller compared to those during summer. Therefore, Noah-MP driven by the GFDL-ESM2G climate with the lowest warming produces the largest annual LAI trends in the Upper and Lower Colorado and Great basin, but the least in the Pacific Northwest, where the vegetation growth is limited by cold climates.

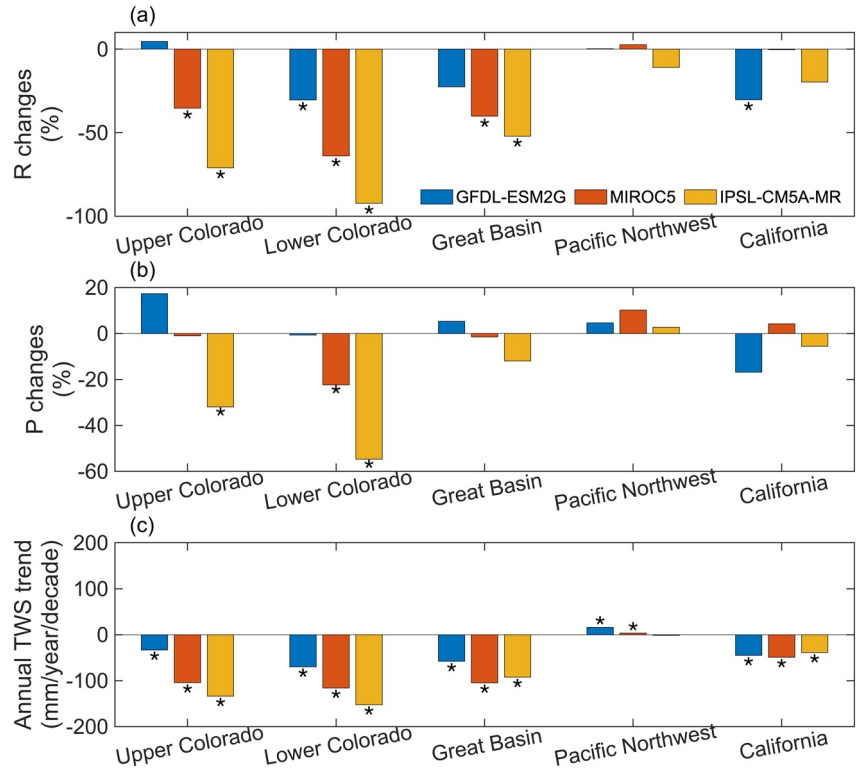

Figure 5. Noah-MP projected (a) runoff change from 2016-2099 (%), (b) precipitation change from 2016-2099 (%), and (c) TWS linear trends (terrestrial water storage; mm/year/decade) for each river driven by different climates produced by the three global climate models. The legend provided in (a) applies to all other parts. The asterisks represent significant trends ($p < 0.05$); the total linear changes in percent are relative to the starting year of the linear fit (i.e., 2016). Precipitation is used as an input to drive Noah-MP.

The annual transpiration (T) is projected to significantly increase across the western US (Figure 6b). The annual transpiration is simulated to increase by up to 68% (8 mm/year/decade), 43% (7 mm/year/decade), 84% (9 mm/year/decade), 51% (10 mm/year/decade), and 30% (8 mm/year/decade) from 2016 to 2099 over the five HUC2 rivers, respectively. The projected ET increases by up to 27% (10 mm/year/decade), 9% (4 mm/year/decade), 20% (6 mm/year/decade), 25% (11 mm/year/decade), and 10% (5 mm/year/decade) from 2016 to 2099 over the five rivers, indicating that transpiration contributes the most to the ET increases. Additionally, the simulated ratio of transpiration to ET (T/ET) shows a significant increasing trend by up to 53% (2%/decade), 44% (2%/decade), 74% (3%/decade), 21% (1%/decade), and 18% (1%/decade) from 2016 to 2099 over the five rivers, respectively. Despite the declining transpiration trend in the Lower Colorado for IPSL-CM5A-MR, the T/ET ratio shows an increasing trend due to decreases in ET. The increasing trend in the T/ET ratio indicates an enhanced WUE under the increasing CO_2 concentration. However, increases in transpiration are not necessarily related to increases in LAI (greening) as reflected from CON-CO2 (Figure 8b; see discussions in Section 3.4).

We conducted an attribution analysis based on the PM equation (see Appendix A), which helps discern the dominant factors contributing to changes in ET. The conceptual PM model represents a "big-leaf" (or a single source) evaporating surface, while Noah-MP represents multiple evaporating sources including soil surface evaporation, interception loss, and transpiration. By fitting the Noah-MP modeled ET with the PM model, a single "surface resistance" (r_s in PM) can be derived. As such, r_s represents a combined effect of resistances of the soil surface, leaf boundary layer, and leaf stomata, reflecting the overall water supply from the land surface given the atmospheric water demand.

We first calculated the multi-year mean of basin-averaged air temperature, pressure and specific humidity, wind speed, surface roughness length, and sensible and latent heat fluxes during 2016–2045 and during 2070–2099. Using these spatiotemporal-averaged values, we calculated the basin-averaged net radiation (R_n), water vapor pressure deficit (vpd), the slope of the saturated water vapor pressure against air temperature (δ), and aerodynam-

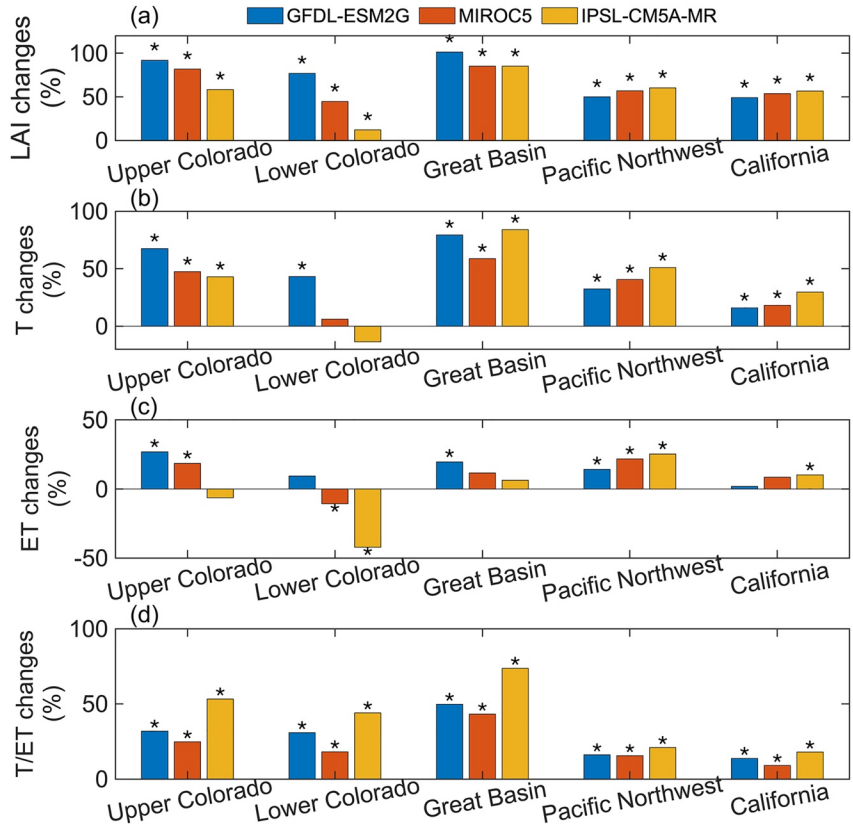

Figure 6. Noah-MP projected total linear changes from 2016 to 2099 relative to the linear fit in 2016 in annual (a) LAI (leaf area index), (b) T (transpiration), (c) ET (evapotranspiration), and (d) T/ET ratio for the two-digital hydrological unit code rivers. The legend provided in (a) applies to all subparts. The asterisks indicate total linear changes pass the significant test ($p < 0.05$).

ic resistance (r_a). The basin-averaged r_s was then derived by fitting the resulting ET from the PM equation with inputs of the basin-averaged R_n, vpd, δ, and r_a against the basin-averaged model outputs of ET during 2016–2045 and 2070–2099. We then quantified the contributions of changes in R_n, vpd, δ, r_a, and r_s (ΔR_n, Δvpd, $\Delta\delta$, Δr_a, and Δr_s in Equation A2) during 2070–2099 averaged over each river basin relative to those during 2016–2045 to the corresponding changes in ET (ΔET in Equation A2; Figure 7).

The ET changes reconstructed through the PM equation from CTRL agree well with the Noah-MP outputs with an r^2 value of 0.98 (Figure 7b), indicating an overall excellent but not perfect fit, more apparently over the Lower Colorado for IPSL-CM5A-MR (the outlier in Figure 7b). The non-perfect fit is most likely caused by (a) averaging, in space and time, ET and its controlling factors in PM, of which the relationships are nonlinear, and (b) the difference between r_a used in PM and the multiple aerodynamic resistances used in Noah-MP. The largest positive contributor to ΔET over all the rivers is Δvpd followed by $\Delta\delta$ due to the nature of the increasing slope of the saturated water vapor pressure against temperature (Figure 7a). ΔR_n also positively contributes to ΔET, and it is due to increased downward longwave radiation (Figure S1 in Supporting Information S1), surface "greening"-induced reduction in surface albedo, and warming-induced surface "darkening" due to shrinking snow cover (Figure 8f; Milly & Dunne, 2020). ΔET due to ΔR_n, Δvpd, and $\Delta\delta$ is the largest for IPSL-CM5A-MR (which produces the strongest warming among the three GCMs), but the lowest for GFDL-ESM2G with a weaker warming, because vpd and δ are strongly dependent on temperature. Due to the slightly slowing winds (Figure S1 in Supporting Information S1), Δr_a plays a negative but negligible role in the ET changes. Increases in r_s, which may include the combined effects of stomatal closure, surface "greening", and soil surface drying, largely reduce ET by −0.35 (mm/day), −0.71 (mm/day), −0.19 (mm/day), −0.15 (mm/day), and −0.20 (mm/day) over river basins 14–18, respectively, representing the largest negative contributor. Because the negative contribution of Δr_s exceeds the combined positive contribution of other variables, ΔET is negative over the Lower Colorado for MIROC5 (Fig-

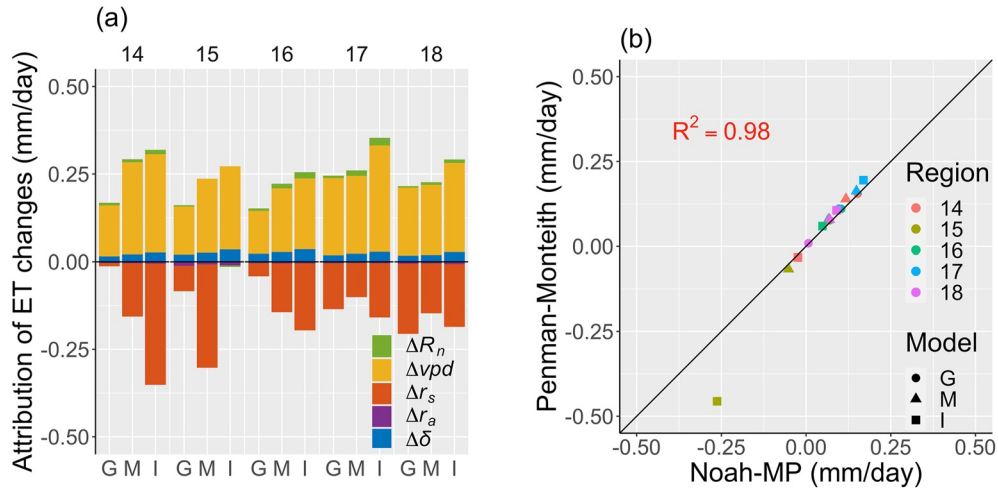

Figure 7. (a) Contribution of ΔR_n, Δvpd, Δr_s, Δr_a, and $\Delta\delta$ to ΔET (2070–2099 relative to 2016–2045); (b) Scatter plot of ΔET during 2070–2099 relative to 2016–2045 resulting from Noah-MP and those computed by the Penman-Monteith equation. G, M, and I represent GFDL-ESM2G, MIROC5, and IPSL-CM5A-MR, respectively.

ure 6c). However, due to the bad fit between the PM-derived and the modeled ET (Figure 7b), this approach fails to explain the ET changes over the Lower Colorado for IPSL-CM5A-MR. From this analysis, it is apparent that Δvpd and Δr_s largely control the future ET changes, suggesting the counteracting effects of the warming-induced increases in the atmospheric demand and the decreasing surface water supply. However, the contribution of Δr_s to ΔET is more complicated due to the soil surface drying and the two counteracting effects of CO_2.

3.4. Compensatory Surface "Greening" and Stomatal Closure Effects

The negative contribution of Δr_s to ΔET can be a combined net effect of plant stomatal closure, surface "greening", and soil surface drying. We assessed the surface "greening" effect through the difference between CTRL and STATIC-LAI and the stomatal closure effect through the difference between CON-CO2 and STATIC-LAI. We first compared some key hydrological variables resulting from CTRL, CON-CO2, and STATIC-LAI over the five rivers (Figure 8) and then conducted a PM-based attribution analysis to quantify the "greening" effect (Figure 9a) and stomatal closure effect (Figure 9b).

STATIC-LAI (without a trend in LAI or "greening" effects) projects a much smaller trend in transpiration (Figure 8b) and ET (Figure 8c) than does CTRL, becoming slightly negative. Consequently, the decreasing runoff trend projected by CTRL is largely reduced due to removal of the "greening" effect in STATIC-LAI. The projected changes in runoff are generally consistent with the changes in TWS (Figure 8e), soil moisture (Figure 8g), and groundwater storage (Figure 8h), all showing reduced decreasing trends. The comparison between CTRL and STATIC-LAI suggests that the surface "greening" plays an important role in the projected changes of transpiration, ET, runoff, and TWS. In addition, STATIC-LAI projects a larger declining trend in SWE (Figure 8f) than does CTRL due likely to less vegetation shading and thus increased solar radiation absorption by the snowpack on the ground.

In CON-CO2, both the "greening" and stomatal closure effects are removed. As a result, the projected LAI trends are largely reduced (Figures 8a and S9 in Supporting Information S1) due to removal of the greening effect. However, CON-CO2 projects a similar level of changes in transpiration (Figure 8b), ET (Figure 8c), runoff (Figure 8d), SWE (Figure 8f), and soil moisture (Figure 8g) to those by CTRL. CON-CO2 projects enhanced runoff reductions in Rivers 17 & 18, because the stomatal closure effect may exceed the impact of surface greening, while Rivers 14–16 showing an opposite case. Because the two counteracting effects of CO_2 are roughly compensatory, CON-CO2 projects changes in hydrological variables that are comparable with CTRL. This suggests that the warming effect remains the largest factor controlling the long-term change in hydrologic processes.

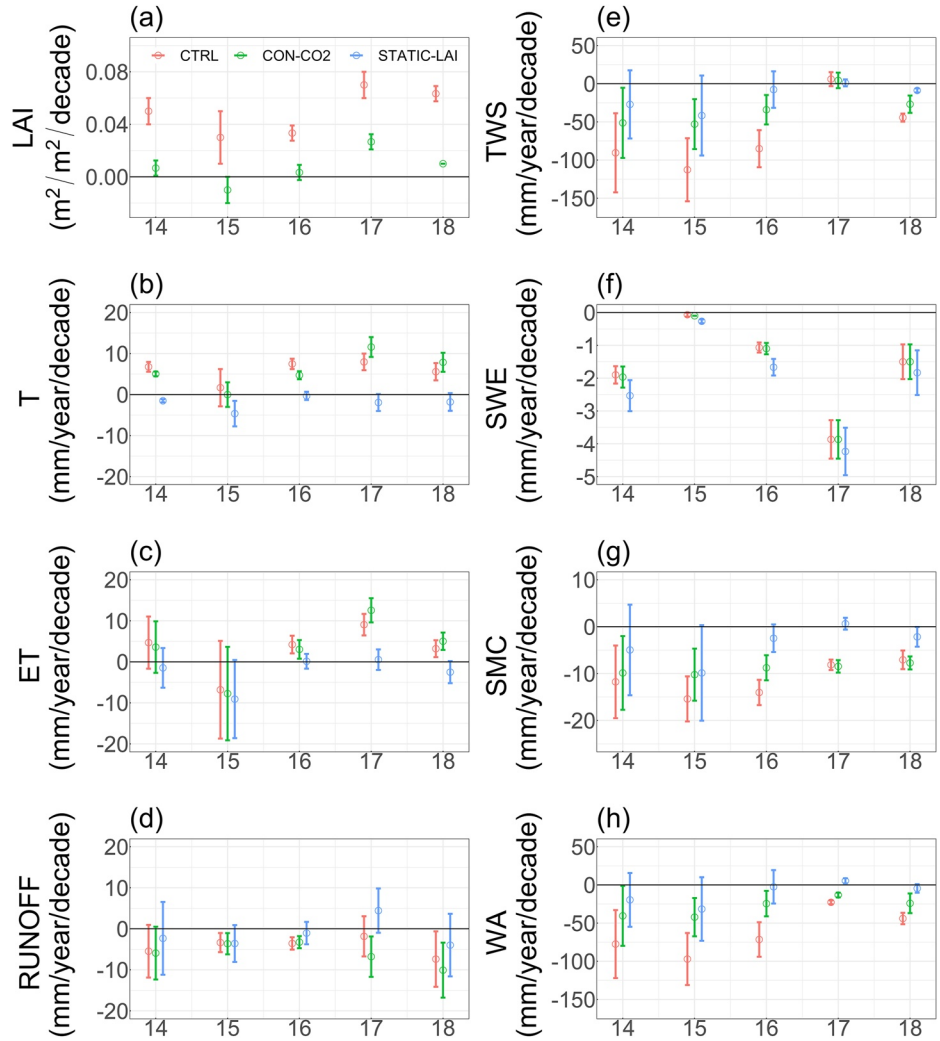

Figure 8. The model projected trends in (a) leaf area index (LAI) (m^2/m^2/decade), (b) transpiration (T; mm/year/decade), (c) evapotranspiration (ET; mm/year/decade), (d) runoff (mm/year/decade), (e) terrestrial water storage (TWS; mm/year/decade), (f) snow water equivalent (SWE; mm/year/decade), (g) soil moisture (SMC; mm/year/decade), and (h) groundwater storage in aquifers (WA; mm/year/decade) by CTRL, CON-CO2, and STATIC-LAI for each two-digital hydrological unit code rivers. The legend provided in (a) applies to all subparts. The circles and error bars represent the ensemble mean of trends and ±1 standard deviation from the three climate models.

We conducted the same PM-based analyses of the two sensitivity experiments: STATIC-LAI (Figure S7 in Supporting Information S1) and CON-CO2 (Figure S8 in Supporting Information S1). We then computed the difference of the ΔET attributions between CTRL and STATIC-LAI (Figure 9a) and that between CON-CO2 and STATIC-LAI (Figure 9b). The effect of Δr_s stands out above all else, becoming the most dominant contributor in both cases, but the former (Figure 9a) indicates the surface greening effect, while the latter (Figure 9b) indicates the stomatal closure effect.

Both STATIC-LAI and CTRL are driven by the increasing RCP 8.5 CO_2 concentration. The difference between CTRL and STATIC-LAI removes the CO_2 effects on stomatal closure but retains only the "greening" effect (Figure 9a). Also, ΔR_n becomes a positive contributor due to the surface greening, which lowers the surface albedo (with negligible effects from changes in snow cover; see Figure 8f). Δr_a can be a positive or negative contributor due possibly to different changes in surface roughness length and zero-displacement height associated with a different extent of greening over various basins under various climates. Δvpd and $\Delta\delta$ contributions to ΔET are

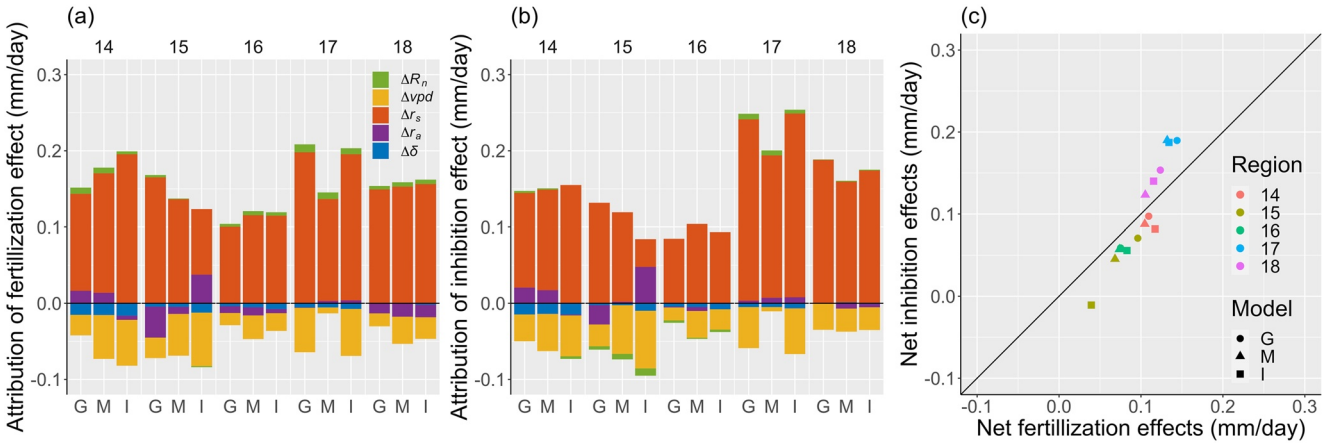

Figure 9. Contribution of ΔR_n, Δvpd, Δr_s, Δr_a, and $\Delta\delta$ to ΔET (2070–2099 relative to 2016–2045). (a) CTRL – STATIC-leaf area index (LAI) (surface "greening" effect), (b) CON-CO2 – STATIC-LAI (stomatal closure effect), and (c) the net stomatal closure (or inhibition) effect versus the net surface "greening" (or fertilization) effect over different rivers and under various climates. The legend provided in (a) applies to (b).

due largely to the smaller first-derivatives of *vpd* and δ because Δvpd and $\Delta\delta$ are the same in CTRL and STATIC-LAI experiments.

CON-CO2 completely removes the stomatal closure effect and largely removes the surface greening effects, because other factors such as changes in radiation, temperature, and humidity may contribute to the greening (Figure 8a), while STATIC-LAI completely removes the greening effect but contains the stomatal closure effect. Thus, the difference between CON-CO2 and STATIC-LAI approximates the stomatal closure effect with the greening effect being mostly removed (Figure 9b). The stomatal closure effect also affects the contribution of changes in Δvpd, $\Delta\delta$, Δr_a, and ΔR_n to ΔET, but with a much smaller magnitude compared to that of Δr_s. The magnitudes of the two counteracting CO_2 effects on ET changes are roughly equal (~0.15 mm/day averaged over all basins and climates, Figure 9c), more than half of the contribution of the warming effects to ET changes, which are dominated by Δvpd (~0.2 mm/day; Figure S8 in Supporting Information S1) in CON-CO2.

Interestingly, the CO_2 fertilization (greening) effect on ET is lower than the stomatal closure effect at lower elevations (<~1,500 m; ~53% of the western US; Figure S10 in Supporting Information S1) but tends to increase, slightly exceeding the stomatal closure effect at higher elevations (>~1,500 m; 47%; Figure 10). Both grasslands and shrublands exhibit a greater greening effect than the stomatal closure effect at all altitudes (Figures S11 &

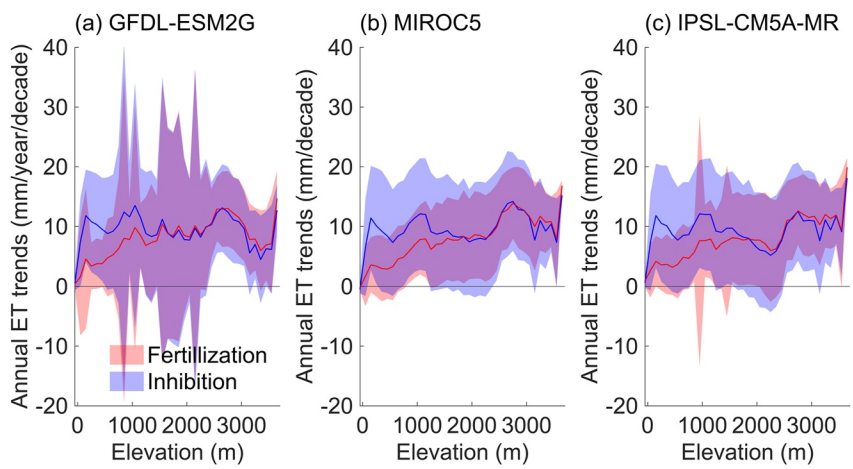

Figure 10. Averaged annual evapotranspiration trend (unit: mm/year/decade; solid lines) for each elevation band (100 m) in the western US with the shaded area representing ± 1 standard deviation for GFDL-ESM2G (a), MIROC5 (b), and IPSL-CM5A-MR (c) models of the CO_2 fertilization (pink) and inhibition (blue) effects. The legend provided in (a) applies to all subparts.

S12 in Supporting Information S1), but the evergreen needleleaf forests show an opposite pattern, more apparently at lower elevations (Figure S13 in Supporting Information S1), dominating the overall pattern in the western US (Figure 10). This is due likely to different plants' response to other abiotic factors (e.g., temperature, humidity, and soil water etc.) beyond elevated CO_2 concentration. More apparently for the shrubs and evergreen needleleaf trees (Figures S12 & S13 in Supporting Information S1), the CO_2 greening effects on ET increase with elevation as they become less water-stressed due likely to the "water tower" effects (Viviroli et al., 2007) and then decline toward the mountain tops (>3000 m) as they become more cold-stressed.

4. Discussions

4.1. Projected Changes in Runoff, Groundwater Storage, and Vegetation

This study was initiated to project future runoff under projected climates following previous studies (e.g., Naz et al., 2016; Sun et al., 2016) but used a different LSM with explicit representations of plant physiological and phenological responses. Overall, the future runoff projected by CTRL declines significantly. Despite the similar conclusions to previous studies, the two sensitivity experiments with Noah-MP reveals the counteracting CO_2 fertilization effects on surface greening and inhibition effects on plant stomatal closure are roughly compensatory. The CON-CO2 experiment is similar to previous studies that did not take CO_2 concentration changes into account. Compared to CTRL, CON-CO_2 projected a similar runoff trend in the Upper and Lower Colorado and Great Basin but a larger reduction in the Pacific Northwest and California (Figure 8d). In other words, the vegetation responses to elevated CO_2 concentration may alleviate the water shortage in the Pacific Northwest and California. In summary, Noah-MP projected aggravating and alleviating CO_2 impacts on runoff in semi-arid and semi-humid regions (Figure 9c), respectively, consistent with previous studies for Australia (Ukkola et al., 2016) and the Jinghe River basin in China (Huang et al., 2019). The water shortage in the semiarid and arid regions is exacerbated partially because elevated CO_2 enhances carbon allocation to roots and results in deeper roots (Nie et al., 2013) and larger root surface area, which benefits root uptake of deeper soil water and increases in transpiration (Trancoso et al., 2017; Y. Yang et al., 2021). These processes are also represented in the Noah-MP version used in this study.

As an important indicator of freshwater resources, changes in TWS including SWE, soil water, and groundwater, are worth further investigation. Noah-MP shows a fairly good ability to reproduce the TWS variations in the historical period from 2002 to 2015 (Figure 4). The analysis of its components indicates that the decrease in TWS, given the future warming, is mainly attributed to the declining groundwater storage (Figures 8e–8h). However, the partitioning of TWS change to changes in the soil water and groundwater components is dependent on the model representations of root dynamics as well as the hydraulic conductivity and matric water potential (or capillary fringe) of the aquifers, which further depends on the structure and texture of deeper soils and aquifers (B. Li, Rodell et al., 2021). Further investigations of the groundwater storage change should be based on model validations against available groundwater level data (Fan et al., 2013).

The projected LAI changes are dominated by CO_2 but influenced by multiple other factors, consistent with previous studies (Mahowald et al., 2016; Mankin et al., 2017). Although the LAI trends are substantially reduced due to the removal of increasing CO_2 trend, nonnegligible LAI trends were still found in all regions (except River 15; Figure 8a). Earlier and longer growing season induced by the warming facilitates the CO_2 fertilization effect on the greening, especially over the colder mountain ridges (Figure S9 in Supporting Information S1). It should be noted that earlier spring greening reduces spring soil moisture, which can persist into the following summer and exacerbate summer soil drying (Lian et al., 2020). On the contrary, the warming and precipitation reductions result in decreases in LAI in the warmer Lower Colorado (River 15) without the CO_2 fertilization effects (CON-CO2; Figure S9 in Supporting Information S1). This highlights the important control of other abiotic factors beyond the CO_2 fertilization effects on the long-term trend in vegetation growth. Increasing specific humidity also slightly alleviates the water stress on carbon assimilation, benefiting vegetation growth and reducing forest mortality risks (Liu et al., 2017).

Since Idso and Brazel (1984), a number of studies have argued the CO_2-induced stomatal closure effects on amelioration of water shortage (Lian et al., 2018; Milly & Dunne, 2016; Roderick et al., 2015; Swann et al., 2016; Y. Yang et al., 2019). Our STATIC-LAI experiment produces negligible changes in transpiration and ET (Figures 8b and 8c), suggesting that the stomatal closure effect can be as large as the warming effect and thereby cancel out

the warming effect. Although the CO_2-induced stomatal closure remarkably reduces transpiration, widespread runoff reductions (though small) are still projected in the future (Figure 8d), highlighting the importance of warming on the hydrologic cycle as shown by the CON-CO2 experiment. However, surface greening mainly due to rising CO_2 has nonnegligible impacts on the hydrological cycle, equivalent to the stomatal closure effects. Our study suggests that the two complementary CO_2 effects should be considered together rather than emphasizing one of them as done in some previous studies (Idso & Brazel, 1984; Mankin et al., 2019; Milly & Dunne, 2016; Y. Yang et al., 2019).

4.2. Uncertainties

In this study, the spatial distribution of vegetation types is prescribed and kept constant during the 100-year simulations under a changing climate. In reality, natural disturbances (Donohue et al., 2017) and human activities may influence the vegetation vigor and species. For example, bark beetle outbreaks and wildfire have resulted in tree mortality in nearly 15% of the forested area across the western US during the past three decades (Hicke et al., 2016). Tree mortality is also projected to likely increase in the future, especially in the southwest US (Buotte et al., 2019; Jiang et al., 2013; Thorne et al., 2018). Jiang et al. (2013) projected that half of the regions dominated by evergreen needleleaf forests in the western US will shift into shrub- and grass-dominant areas by the end of the 21st century under the "business-as-usual" emission scenario (A2 in the IPCC Assessment Report 4). These potential vegetation changes may increase or reduce runoff by altering the hydrologic cycle (Goeking & Tarboton, 2020). Although the forested area comprises less than 20% of the western US, future work should better understand the impacts of these disturbances on water resources.

Another source of uncertainties is the T/ET ratio, which is very uncertain due to a lack of direct transpiration observations and thus limited understanding of the vegetation physiological processes. Because of the scarcity of large-scale transpiration observations and accurate ET products, we relied on observational datasets of the USGS monthly runoff and GRACE TWSA, of which the seasonal variations and trends largely represent the cumulative effects of ET, in the calibration. However, Lian et al. (2018) found that the simulated global T/ET ratio by CMIP5 ESMs tends to be lower than *in-situ* observations, indicating that the vegetation would probably play a more important role in future runoff change. They attributed this underestimation to inadequate representations of canopy light use, interception loss, and root water uptake. Noah-MP, like many other LSMs, struggles to simulate a T/ET ratio lower than observations (Figure S14 in Supporting Information S1), indicating that the vegetation contribution to ET (Zeng et al., 2017; Y. Zhang et al., 2016) and thus runoff changes may be underestimated. The low T/ET ratio produced by Noah-MP and other LSMs may be caused by a lack of adequate representations of lateral water flow and water vapor diffusion within the surface soil pores (Chang et al., 2018). Overall, the limited understanding of vegetation dynamics constrains us from better projecting the ecosystem responses to an unprecedent future climate. To reduce these uncertainties, large-scale observations and controlled experiments are required.

Uncertainties also exist in the validation datasets and downscaling processes. The MODIS LAI product is mainly generated through MODIS reflectance data, a look-up table, and a three-dimensional radiation transfer model (Yan et al., 2016). Uncertainties in the observed LAI tend to be high in regions with dense canopy cover and complex terrain. Therefore, this may explain the relatively high negative model biases in the Pacific Northwest coastal regions and the Cascades. Moreover, the water balance for some grid cells may be not closed because of different sources of validation datasets (Cai et al., 2014; Zheng et al., 2020). For instance, over the Lower Colorado, the observed precipitation, runoff, ET, and TWS change are not well balanced. For this reason, Noah-MP overestimated both runoff and ET due to overestimated precipitation input. Additionally, despite the good performance of the linear regression approach in correcting the biases in the CMIP5 data, this method may reduce the interannual variabilities of the variables and usually neglect the dynamic atmospheric processes induced by subgrid variations in topography and land cover (Xue et al., 2014), compared to dynamic downscaling.

Uncertainties in model structure (process parameterizations) and parameters may also produce biases in the trend. LSMs may show a wide range of future runoff changes under climate change and elevated CO_2 in some regions (Davie et al., 2013). The large spread of model projections potentially comes from various simplified and incomplete representations of bio-geophysical processes affecting ET. This is also why we used a Noah-MP version that enhanced the plant drought resilience through representations of dynamic root water uptake and groundwater capillary rise enhance, thereby surviving more frequent droughts given the future warming (Niu et al., 2020). Other model components, such as carbon allocation and respiration schemes (Mankin et al., 2017),

also affect the extent of vegetation greening. Most current LSMs, including Noah-MP, likely overestimate the greening trends due to incomplete understandings of the vegetation processes, such as nutrient limitations and interactions between roots and microbes (Smith et al., 2016). In addition, prescribed model parameters can result in additional uncertainties depending on the parameter sensitivity (Chaney et al., 2016; Cuntz et al., 2016). In this study, we used a Noah-MP version that are manually optimized (see more details in Niu et al., 2020) and validated over historical periods (Figures 2–4 and Figures S3–S5 in Supporting Information S1). However, the search of optimum parameter values may be incomplete, and some key model parameters are constant for the whole model domain, for example, the decay factor of groundwater discharge (or baseflow). To reduce the modeling uncertainty from parameter values, combining sensitivity analyses with machine learning (Chaney et al., 2016) and model selection techniques (X. Zhang et al., 2014) may represent a way forward despite the expensive computational cost (Huo et al., 2019). We hope this study would inspire more future studies on the vegetation responses to elevated CO_2 concentration using different models with different process representations while considering parameter uncertainties.

5. Conclusion

This study aimed to improve the understanding of the impacts of terrestrial ecosystems response to rising CO_2 on terrestrial water resources across the western US river basins through projections of runoff under different warming climates projected by three GCMs under RCP 8.5. We used the mechanistic Noah-MP LSM with explicit representations of plant physiological and structural responses to the CO_2 inhibition effect on stomatal opening (stomatal closure) and fertilization effect on photosynthesis (surface "greening"). The good performance of Noah-MP in comparison with observations (Figures 2–4 and Figures S3–S5 in Supporting Information S1) gives us some confidence in the projected changes in the 21st Century. The relatively worse model performance over the Lower Colorado River is due mainly to the overestimated precipitation input. Through sensitivity experiments and PM-based attribution analyses, we conclude that:

1. The projected annual runoff shows a widespread decline over the Upper Colorado, Great Basin, Pacific Northwest, and California by −71%, −52%, −11%, and −30% from 2016 to 2099, respectively, due mainly to increases in ET, and over the Lower Colorado by −92% but due mainly to decreases in precipitation.
2. Both the stomatal closure and surface "greening" effects represent the second largest contributor to the projected increases in ET following the warming effect. The PM-based analysis indicates that the increasing atmospheric demand (through increases in *vpd* and δ) plays a dominant role over the increasing available energy (through changes in R_n) due to increases in downward longwave radiation, surface "greening" (increases in LAI), and surface "darkening" (due to shrinking snow cover).
3. The two counteracting effects of surface "greening" and stomatal closure are roughly compensatory at the HUC2 river basin scale, and therefore the projected changes in ET and runoff under RCP 8.5 (CTRL) show a magnitude of change similar to those with constant CO_2 concentration (CON-CO2) across the western US HUC2 rivers. However, the strength of the two effects are dependent on vegetation types distributing over different elevation bands, with the stomatal closure effect exceeding the "greening" effect for evergreen needleleaf forests over low elevation bands (<∼1,500 m).

This study suggests that both the surface "greening" and stomatal closure effects are important factors and should be considered together in runoff and water availability projections. In contrast, projections with prescribed LAI seasonal cycle without year-to-year variations (i.e., without the "greening" effect) would lead to misleading results.

Appendix A

We quantified the attribution of ET changes based on the Penman-Monteith equation (Monteith, 1965).

$$\lambda \mathrm{ET} = \frac{\delta R_n + \rho_a C_p vpd / r_a}{\delta + \gamma(1 + r_s / r_a)} \tag{A1}$$

where λ is the latent heat of vapourization (J/kg); ET is the evaporation flux (kg/(m^2/s)); δ is the slope of the saturation vapor pressure-temperature relationship (Pa/K); R_n is the total available energy (equivalent to the sum of

sensible and latent heat fluxes; W/m^2); ρ_a is the air density (kg/m^3); C_p is the specific heat of air (J/(kg/K)); *vpd* is the vapor pressure deficit of the air (Pa); γ is the psychrometric constant (Pa/K); r_a is the aerodynamic resistance (s/m); and r_s is the surface resistance (s/m).

The change in ET can be approximated as the sum of ET changes caused by changes in R_n, *vpd*, r_s, r_a, and δ, following Y. Yang et al. (2019), Ban et al. (2020), and Neto et al. (2020):

$$\Delta \mathrm{ET} \approx \frac{\partial \mathrm{ET}}{\partial R_n}\Delta R_n + \frac{\partial \mathrm{ET}}{\partial vpd}\Delta vpd + \frac{\partial \mathrm{ET}}{\partial r_s}\Delta r_s + \frac{\partial \mathrm{ET}}{\partial r_a}\Delta r_a + \frac{\partial \mathrm{ET}}{\partial \delta}\Delta \delta \tag{A2}$$

where the first derivatives of the five dependent variables in Equation A2 are as follows:

$$\frac{\partial \mathrm{ET}}{\partial R_n} = \frac{\delta}{\gamma[\delta + \gamma(1 + \frac{r_s}{r_a})]} \tag{A3}$$

$$\frac{\partial \mathrm{ET}}{\partial vpd} = \frac{\rho_a C_p}{\lambda r_a[\delta + \gamma(1 + \frac{r_s}{r_a})]} \tag{A4}$$

$$\frac{\partial \mathrm{ET}}{\partial r_s} = \frac{-\gamma[\delta R_n + \frac{\rho_a C_p vpd}{r_a}]}{\lambda r_a[\delta + \gamma(1 + \frac{r_s}{r_a})]^2} \tag{A5}$$

$$\frac{\partial \mathrm{ET}}{\partial r_a} = \frac{\gamma r_s[\delta R_n + \frac{\rho_a C_p vpd}{r_a}]}{\lambda {r_a}^2[\delta + \gamma(1 + \frac{r_s}{r_a})]^2} - \frac{\rho_a C_p vpd}{\lambda {r_a}^2[\delta + \gamma(1 + \frac{r_s}{r_a})]} \tag{A6}$$

$$\frac{\partial \mathrm{ET}}{\partial \delta} = \frac{R_n}{\lambda[\delta + \gamma(1 + \frac{r_s}{r_a})]} - \frac{\delta R_n + \frac{\rho_a C_p vpd}{r_a}}{\lambda[\delta + \gamma(1 + \frac{r_s}{r_a})]^2} \tag{A7}$$

Data Availability Statement

The data used in this study are all available online: NLDAS-2 data (http://www.emc.ncep.noaa.gov/mmb/nldas/); the 1-km hybrid State Soil Geographic Database and the USGS 24-category vegetation data (https://ral.ucar.edu/solutions/products/noah-multiparameterization-land-surface-model-noah-mp-lsm); the monthly USGS Water Watch hydrological unit runoff data (https://waterwatch.usgs.gov/); the FLUXNET-MTE GPP and latent heat flux data (https://www.bgc-jena.mpg.de/bgi/index.php/Services/Overview); the MODIS LAI data (http://global-change.bnu.edu.cn/research/laiv6); the GRACE TWSA data (http://grace.jpl.nasa.gov); the University of Arizona SWE data (https://nsidc.org/data/nsidc-0719/versions/1); the CMIP5 model outputs (https://esgf-node.llnl.gov/search/cmip5/); the future CO_2 concentration data under RCP8.5 (https://pcmdi.llnl.gov/mips/cmip5/forcing.html); and the daily precipitation of MACAv2-METDATA (https://climate.northwestknowledge.net/MACA/).

Acknowledgments
This research project was funded by the NASA MAP Program (80NSSC17K0352), NOAA OAR's OWAQ (NA18OAR4590397), DOE Earth System Modeling Program (DE-AC52-498 07NA27344/B639244), and the Strategic Environmental Research and Development Program (SERDP) of the US Department of Defense awarded to Charles P. Hawkins as the lead Principal Investigator (RC18-1034). We thank the editorial team and two anonymous reviewers for the insightful comments that significantly improved the presentation of our work.

References

Abatzoglou, J. T. (2013). Development of gridded surface meteorological data for ecological applications and modelling. *International Journal of Climatology*, *33*(1), 121–131. https://doi.org/10.1002/joc.3413

Ahlström, A., Raupach, M. R., Schurgers, G., Smith, B., Arneth, A., Jung, M., et al. (2015). The dominant role of semi-arid ecosystems in the trend and variability of the land CO_2 sink. *Science*, *348*(6237), 895–899. https://doi.org/10.1126/science.aaa1668

Andela, N., Liu, Y., van Dijk, A. I. J. M., De Jeu, R., & McVicar, T. (2013). Global changes in dryland vegetation dynamics (1988–2008) assessed by satellite remote sensing: Comparing a new passive microwave vegetation density record with reflective greenness data. *Biogeosciences*, *10*(10), 6657–6676. https://doi.org/10.5194/bg-10-6657-2013

Anderson, M., & Woosley, L. (2006). Water availability for the Western United States—Key scientific challenges. Circular 1261. Washington, DC: *US Geological Survey*.

Ashfaq, M., Ghosh, S., Kao, S. C., Bowling, L. C., Mote, P., Touma, D., et al. (2013). Near-term acceleration of hydroclimatic change in the western US. *Journal of Geophysical Research: Atmospheres*, *118*(19), 10676–10693. https://doi.org/10.1002/jgrd.50816

Ball, J. T., Woodrow, I. E., & Berry, J. A. (1987). A model predicting stomatal conductance and its contribution to the control of photosynthesis under different environmental conditions. In *Progress in photosynthesis research* (pp. 221–224). Springer. https://doi.org/10.1007/978-94-017-0519-6_48

Ban, Z., Das, T., Cayan, D., Xiao, M., & Lettenmaier, D. P. (2020). Understanding the asymmetry of annual streamflow responses to seasonal warming in the western United States. *Water Resources Research*, *56*(12), e2020WR027158. https://doi.org/10.1029/2020WR027158

Brakebill, J. W., Wolock, D. M., & Terziotti, S. (2011). Digital hydrologic networks supporting applications related to spatially referenced regression modeling 1. *Journal of the American Water Resources Association*, *47*(5), 916–932. https://doi.org/10.1111/j.1752-1688.2011.00578.x

Broxton, P. D., Dawson, N., & Zeng, X. (2016). Linking snowfall and snow accumulation to generate spatial maps of SWE and snow depth. *Earth and Space Science*, *3*(6), 246–256. https://doi.org/10.1002/2016EA000174

Buotte, P. C., Levis, S., Law, B. E., Hudiburg, T. W., Rupp, D. E., & Kent, J. J. (2019). Near-future forest vulnerability to drought and fire varies across the western United States. *Global Change Biology*, *25*(1), 290–303. https://doi.org/10.1111/gcb.14490

Cai, X., Yang, Z. L., Xia, Y., Huang, M., Wei, H., Leung, L. R., & Ek, M. B. (2014). Assessment of simulated water balance from Noah, Noah-MP, CLM, and VIC over CONUS using the NLDAS test bed. *Journal of Geophysical Research: Atmospheres*, *119*(24), 13751–13770. https://doi.org/10.1002/2014JD022113

Chaney, N. W., Herman, J. D., Ek, M. B., & Wood, E. F. (2016). Deriving global parameter estimates for the Noah land surface model using FLUXNET and machine learning. *Journal of Geophysical Research: Atmospheres*, *121*(22), 13218–13235. https://doi.org/10.1002/2016JD024821

Chang, L. L., Dwivedi, R., Knowles, J. F., Fang, Y. H., Niu, G. Y., Pelletier, J. D., et al. (2018). Why do large-scale land surface models produce a low ratio of transpiration to evapotranspiration? *Journal of Geophysical Research: Atmospheres*, *123*(17), 9109–9130. https://doi.org/10.1029/2018JD029159

Chang, L. L., Yuan, R., Gupta, H. V., Winter, C. L., & Niu, G. Y. (2020). Why is the terrestrial water storage in dryland regions declining? A perspective based on gravity Recovery and climate experiment satellite observations and Noah land surface model with multiparameterization schemes model simulations. *Water Resources Research*, *56*(11), e2020WR027102. https://doi.org/10.1029/2020WR027102

Cho, E., Jacobs, J. M., & Vuyovich, C. M. (2020). The value of long-term (40 years) airborne gamma radiation SWE record for evaluating three observation-based gridded SWE data sets by seasonal snow and land cover classifications. *Water Resources Research*, *56*(1), e2019WR025813. https://doi.org/10.1029/2019WR025813

Clow, D. W. (2010). Changes in the timing of snowmelt and streamflow in Colorado: A response to recent warming. *Journal of Climate*, *23*(9), 2293–2306. https://doi.org/10.1175/2009JCLI2951.1

Collatz, G. J., Ribas-Carbo, M., & Berry, J. (1992). Coupled photosynthesis-stomatal conductance model for leaves of C4 plants. *Functional Plant Biology*, *19*(5), 519–538. https://doi.org/10.1071/PP9920519

Cuntz, M., Mai, J., Samaniego, L., Clark, M., Wulfmeyer, V., Branch, O., et al. (2016). The impact of standard and hard-coded parameters on the hydrologic fluxes in the Noah-MP land surface model. *Journal of Geophysical Research: Atmospheres*, *121*(18), 10676–10700. https://doi.org/10.1002/2016JD025097

Davie, J., Falloon, P., Kahana, R., Dankers, R., Betts, R., Portmann, F., et al. (2013). Comparing projections of future changes in runoff from hydrological and biome models in ISI-MIP. *Earth System Dynamics*, *4*(2), 359–374. https://doi.org/10.5194/esd-4-359-2013

Dawson, N., Broxton, P., & Zeng, X. (2017). A new snow density parameterization for land data initialization. *Journal of Hydrometeorology*, *18*(1), 197–207. https://doi.org/10.1175/JHM-D-16-0166.1

Dettinger, M. D., Cayan, D. R., Meyer, M. K., & Jeton, A. E. (2004). Simulated hydrologic responses to climate variations and change in the Merced, Carson, and American River basins, Sierra Nevada, California, 1900–2099. *Climatic Change*, *62*(1–3), 283–317. https://doi.org/10.1023/B:CLIM.0000013683.13346.4f

Dickinson, R. E., Shaikh, M., Bryant, R., & Graumlich, L. (1998). Interactive canopies for a climate model. *Journal of Climate*, *11*(11), 2823–2836. https://doi.org/10.1175/1520-0442(1998)011<2823:ICFACM>2.0.CO;2

Donohue, R. J., Roderick, M. L., McVicar, T. R., & Farquhar, G. D. (2013). Impact of CO_2 fertilization on maximum foliage cover across the globe's warm, arid environments. *Geophysical Research Letters*, *40*(12), 3031–3035. https://doi.org/10.1002/grl.50563

Donohue, R. J., Roderick, M. L., McVicar, T. R., & Yang, Y. (2017). A simple hypothesis of how leaf and canopy-level transpiration and assimilation respond to elevated CO_2 reveals distinct response patterns between disturbed and undisturbed vegetation. *Journal of Geophysical Research: Biogeosciences*, *122*(1), 168–184. https://doi.org/10.1002/2016JG003505

Easterling, D. R., Arnold, J., Knutson, T., Kunkel, K., LeGrande, A., Leung, L. R., et al. (2017). Precipitation change in the United States. In *Climate science special report: Fourth national climate assessment* (pp. 207–230). U.S. Global Change Research Program.

Fan, Y., Clark, M., Lawrence, D. M., Swenson, S., Band, L., Brantley, S. L., et al. (2019). Hillslope hydrology in global change research and Earth system modeling. *Water Resources Research*, *55*(2), 1737–1772. https://doi.org/10.1029/2018WR023903

Fan, Y., Li, H., & Miguez-Macho, G. (2013). Global patterns of groundwater table depth. *Science*, *339*(6122), 940–943. https://doi.org/10.1126/science.1229881

Farquhar, G. D., von Caemmerer, S., & Berry, J. A. (1980). A biochemical model of photosynthetic CO_2 assimilation in leaves of C_3 species. *Planta*, *149*(1), 78–90. https://doi.org/10.1007/BF00386231

Fensholt, R., Langanke, T., Rasmussen, K., Reenberg, A., Prince, S. D., Tucker, C., et al. (2012). Greenness in semi-arid areas across the globe 1981–2007—An Earth observing satellite based analysis of trends and drivers. *Remote Sensing of Environment*, *121*, 144–158. https://doi.org/10.1016/j.rse.2012.01.017

Field, C. B., Jackson, R. B., & Mooney, H. A. (1995). Stomatal responses to increased CO_2: Implications from the plant to the global scale. *Plant, Cell and Environment*, *18*(10), 1214–1225. https://doi.org/10.1111/j.1365-3040.1995.tb00630.x

Forbes, W. L., Mao, J., Jin, M., Kao, S.-C., Fu, W., Shi, X., et al. (2018). Contribution of environmental forcings to US runoff changes for the period 1950–2010. *Environmental Research Letters*, *13*(5), 054023. https://doi.org/10.1088/1748-9326/aabb41

Frank, D., Poulter, B., Saurer, M., Esper, J., Huntingford, C., Helle, G., et al. (2015). Water-use efficiency and transpiration across European forests during the Anthropocene. *Nature Climate Change*, *5*(6), 579–583. https://doi.org/10.1038/nclimate2614

Goeking, S. A., & Tarboton, D. G. (2020). Forests and water yield: A synthesis of disturbance effects on streamflow and snowpack in western coniferous forests. *Journal of Forestry*, *118*(2), 172–192. https://doi.org/10.1093/jofore/fvz069

Hamlet, A. F., & Lettenmaier, D. P. (1999). Effects of climate change on hydrology and water resources in the Columbia River Basin 1. *JAWRA Journal of the American Water Resources Association*, *35*(6), 1597–1623. https://doi.org/10.1111/j.1752-1688.1999.tb04240.x

Hamlet, A. F., Mote, P. W., Clark, M. P., & Lettenmaier, D. P. (2007). Twentieth-century trends in runoff, evapotranspiration, and soil moisture in the western United States. *Journal of Climate*, *20*(8), 1468–1486. https://doi.org/10.1175/JCLI4051.1

Hicke, J. A., Meddens, A. J., & Kolden, C. A. (2016). Recent tree mortality in the western United States from bark beetles and forest fires. *Forest Science*, *62*(2), 141–153. https://doi.org/10.5849/forsci.15-086

Huang, R., Chen, X., & Hu, Q. (2019). Changes in vegetation and surface water balance at basin-scale in Central China with rising atmospheric CO_2. *Climatic Change*, *155*(3), 437–454. https://doi.org/10.1007/s10584-019-02475-w

Huo, X., Gupta, H., Niu, G. Y., Gong, W., & Duan, Q. (2019). Parameter sensitivity analysis for computationally intensive spatially distributed dynamical environmental systems models. *Journal of Advances in Modeling Earth Systems*, *11*(9), 2896–2909. https://doi.org/10.1029/2018MS001573

Idso, S., & Brazel, A. (1984). Rising atmospheric carbon dioxide concentrations may increase streamflow. *Nature*, *312*(5989), 51–53. https://doi.org/10.1038/312051a0

Jiang, X., Rauscher, S. A., Ringler, T. D., Lawrence, D. M., Williams, A. P., Allen, C. D., et al. (2013). Projected future changes in vegetation in western North America in the twenty-first century. *Journal of Climate*, *26*(11), 3671–3687. https://doi.org/10.1175/JCLI-D-12-00430.1

Jung, M., Reichstein, M., Margolis, H. A., Cescatti, A., Richardson, A. D., Arain, M. A., et al. (2011). Global patterns of land-atmosphere fluxes of carbon dioxide, latent heat, and sensible heat derived from eddy covariance, satellite, and meteorological observations. *Journal of Geophysical Research*, *116*(G3), G00J07. https://doi.org/10.1029/2010JG001566

Kennedy, D., Swenson, S., Oleson, K. W., Lawrence, D. M., Fisher, R., Lola da Costa, A. C., & Gentine, P. (2019). Implementing plant hydraulics in the community land model, version 5. *Journal of Advances in Modeling Earth Systems*, *11*(2), 485–513. https://doi.org/10.1029/2018MS001500

Landerer, F. W., & Swenson, S. (2012). Accuracy of scaled GRACE terrestrial water storage estimates. *Water Resources Research*, *48*(4), W04531. https://doi.org/10.1029/2011WR011453

Lemordant, L., Gentine, P., Swann, A. S., Cook, B. I., & Scheff, J. (2018). Critical impact of vegetation physiology on the continental hydrologic cycle in response to increasing CO_2. *Proceedings of the National Academy of Sciences*, *115*(16), 4093–4098. https://doi.org/10.1073/pnas.1720712115

Li, B., Rodell, M., Peters-Lidard, C., Erlingis, J., Kumar, S., & Mocko, D. (2021). Groundwater recharge estimated by land surface models: An evaluation in the conterminous United States. *Journal of Hydrometeorology*, *22*(2), 499–522. https://doi.org/10.1175/JHM-D-20-0130.1

Li, L., Yang, Z. L., Matheny, A. M., Zheng, H., Swenson, S. C., Lawrence, D. M., et al. (2021). Representation of plant hydraulics in the Noah-MP land surface model: Model development and multi-scale evaluation. *Journal of Advances in Modeling Earth Systems*, *13*, e2020MS002214. https://doi.org/10.1029/2020MS002214

Lian, X., Piao, S., Huntingford, C., Li, Y., Zeng, Z., Wang, X., et al. (2018). Partitioning global land evapotranspiration using CMIP5 models constrained by observations. *Nature Climate Change*, *8*(7), 640–646. https://doi.org/10.1038/s41558-018-0207-9

Lian, X., Piao, S., Li, L. Z., Li, Y., Huntingford, C., Ciais, P., et al. (2020). Summer soil drying exacerbated by earlier spring greening of northern vegetation. *Science Advances*, *6*(1), eaax0255. https://doi.org/10.1126/sciadv.aax0255

Liu, Y., Parolari, A. J., Kumar, M., Huang, C.-W., Katul, G. G., & Porporato, A. (2017). Increasing atmospheric humidity and CO_2 concentration alleviate forest mortality risk. *Proceedings of the National Academy of Sciences*, *114*(37), 9918–9923. https://doi.org/10.1073/pnas.1704811114

Ma, N., Niu, G. Y., Xia, Y., Cai, X., Zhang, Y., Ma, Y., & Fang, Y. (2017). A systematic evaluation of Noah-MP in simulating land-atmosphere energy, water, and carbon exchanges over the continental United States. *Journal of Geophysical Research: Atmospheres*, *122*(22), 12245–12268. https://doi.org/10.1002/2017JD027597

Mahowald, N., Lo, F., Zheng, Y., Harrison, L., Funk, C., Lombardozzi, D., & Goodale, C. (2016). Projections of leaf area index in earth system models. *Earth System Dynamics (Online)*, *7*(1), 211–229. https://doi.org/10.5194/esd-7-211-2016

Mankin, J. S., Seager, R., Smerdon, J. E., Cook, B. I., & Williams, A. P. (2019). Mid-latitude freshwater availability reduced by projected vegetation responses to climate change. *Nature Geoscience*, *12*(12), 983–988. https://doi.org/10.1038/s41561-019-0480-x

Mankin, J. S., Smerdon, J. E., Cook, B. I., Williams, A. P., & Seager, R. (2017). The curious case of projected twenty-first-century drying but greening in the American West. *Journal of Climate*, *30*(21), 8689–8710. https://doi.org/10.1175/JCLI-D-17-0213.1

Mao, J., Shi, X., Thornton, P. E., Hoffman, F. M., Zhu, Z., & Myneni, R. B. (2013). Global latitudinal-asymmetric vegetation growth trends and their driving mechanisms: 1982–2009. *Remote Sensing*, *5*(3), 1484–1497. https://doi.org/10.3390/rs5031484

McVicar, T. R., Roderick, M. L., Donohue, R. J., Li, L. T., Van Niel, T. G., Thomas, A., et al. (2012). Global review and synthesis of trends in observed terrestrial near-surface wind speeds: Implications for evaporation. *Journal of Hydrology*, *416*, 182–205. https://doi.org/10.1016/j.jhydrol.2011.10.024

Milly, P. C., & Dunne, K. A. (2016). Potential evapotranspiration and continental drying. *Nature Climate Change*, *6*(10), 946–949. https://doi.org/10.1038/nclimate3046

Milly, P. C., & Dunne, K. A. (2017). A hydrologic drying bias in water-resource impact analyses of anthropogenic climate change. *JAWRA Journal of the American Water Resources Association*, *53*(4), 822–838. https://doi.org/10.1111/1752-1688.12538

Milly, P. C., & Dunne, K. A. (2020). Colorado River flow dwindles as warming-driven loss of reflective snow energizes evaporation. *Science*, *367*(6483), 1252–1255. https://doi.org/10.1126/science.aay9187

Monteith, J. L. (1965). *Evaporation and environment. paper presented at Symposia of the society for experimental biology*. Cambridge University Press (CUP) Cambridge.

Mueller, B., Seneviratne, S. I., Jimenez, C., Corti, T., Hirschi, M., Balsamo, G., et al. (2011). Evaluation of global observations-based evapotranspiration datasets and IPCC AR4 simulations. *Geophysical Research Letters*, *38*(6), L06402. https://doi.org/10.1029/2010GL046230

Naz, B. S., Kao, S.-C., Ashfaq, M., Rastogi, D., Mei, R., & Bowling, L. C. (2016). Regional hydrologic response to climate change in the conterminous United States using high-resolution hydroclimate simulations. *Global and Planetary Change*, *143*, 100–117. https://doi.org/10.1016/j.gloplacha.2016.06.003

Neto, A. A. M., Niu, G.-Y., Roy, T., Tyler, S., & Troch, P. A. (2020). Interactions between snow cover and evaporation lead to higher sensitivity of streamflow to temperature. *Communications Earth & Environment*, *1*(1), 1–7. https://doi.org/10.1038/s43247-020-00056-9

Nie, M., Lu, M., Bell, J., Raut, S., & Pendall, E. (2013). Altered root traits due to elevated CO_2: A meta-analysis. *Global Ecology and Biogeography*, *22*, 1095–1105. https://doi.org/10.1111/geb.12062

Niu, G. Y., Fang, Y. H., Chang, L. L., Jin, J., Yuan, H., & Zeng, X. (2020). Enhancing the Noah-MP ecosystem response to droughts with an explicit representation of plant water storage supplied by dynamic root water uptake. *Journal of Advances in Modeling Earth Systems*, *12*, e2020MS002062. https://doi.org/10.1029/2020MS002062

Niu, G. Y., Yang, Z. L., Dickinson, R. E., & Gulden, L. E. (2005). A simple TOPMODEL-based runoff parameterization (SIMTOP) for use in global climate models. *Journal of Geophysical Research*, *110*(D21), D21106. https://doi.org/10.1029/2005JD006111

Niu, G. Y., Yang, Z. L., Dickinson, R. E., Gulden, L. E., & Su, H. (2007). Development of a simple groundwater model for use in climate models and evaluation with gravity recovery and climate experiment data. *Journal of Geophysical Research*, *112*(D7), D07103. https://doi.org/10.1029/2006JD007522

Niu, G. Y., Yang, Z. L., Mitchell, K. E., Chen, F., Ek, M. B., Barlage, M., et al. (2011). The community Noah land surface model with multiparameterization options (Noah-MP): 1. Model description and evaluation with local-scale measurements. *Journal of Geophysical Research*, *116*(D12), D12109. https://doi.org/10.1029/2010JD015139

Parton, W., Singh, J., & Coleman, D. (1978). A model of production and turnover of roots in shortgrass prairie. *Journal of Applied Ecology*, 515–541. https://doi.org/10.2307/2402608

Prather, M., Flato, G., Friedlingstein, P., Jones, C., Lamarque, J., Liao, H., & Rasch, P. (2013). Annex II: Climate system scenario tables. *Climate Change*, 1395–1445.

Roderick, M. L., Greve, P., & Farquhar, G. D. (2015). On the assessment of aridity with changes in atmospheric CO_2. *Water Resources Research*, *51*(7), 5450–5463. https://doi.org/10.1002/2015WR017031

Sakaguchi, K., & Zeng, X. (2009). Effects of soil wetness, plant litter, and under-canopy atmospheric stability on ground evaporation in the community land model (CLM3.5). *Journal of Geophysical Research*, *114*(D1), D01107. https://doi.org/10.1029/2008JD010834

Sakumura, C., Bettadpur, S., & Bruinsma, S. (2014). Ensemble prediction and intercomparison analysis of GRACE time-variable gravity field models. *Geophysical Research Letters*, *41*(5), 1389–1397. https://doi.org/10.1002/2013GL058632

Seaber, P. R., Kapinos, F. P., & Knapp, G. L. (1987). Hydrologic unit maps. *U. S. Geological Survey Water-Supply Paper*, *2294*, 1–66.

Sheffield, J., Wood, E. F., & Roderick, M. L. (2012). Little change in global drought over the past 60 years. *Nature*, *491*(7424), 435–438. https://doi.org/10.1038/nature11575

Singh, A., Kumar, S., Akula, S., Lawrence, D. M., & Lombardozzi, D. L. (2020). Plant growth nullifies the effect of increased water-use efficiency on streamflow under elevated CO_2 in the Southeastern United States. *Geophysical Research Letters*, *47*(4), e2019GL086940. https://doi.org/10.1029/2019GL086940

Smith, W. K., Reed, S. C., Cleveland, C. C., Ballantyne, A. P., Anderegg, W. R., Wieder, W. R., et al. (2016). Large divergence of satellite and Earth system model estimates of global terrestrial CO_2 fertilization. *Nature Climate Change*, *6*(3), 306–310. https://doi.org/10.1038/nclimate2879

Sun, S., Sun, G., Mack, E. C., McNulty, S., Caldwell, P. V., Duan, K., & Zhang, Y. (2016). Projecting water yield and ecosystem productivity across the United States by linking an ecohydrological model to WRF dynamically downscaled climate data. *Hydrology and Earth System Sciences*, *20*(2), 935–952. https://doi.org/10.5194/hess-20-935-2016

Swann, A. L., Hoffman, F. M., Koven, C. D., & Randerson, J. T. (2016). Plant responses to increasing CO_2 reduce estimates of climate impacts on drought severity. *Proceedings of the National Academy of Sciences*, *113*(36), 10019–10024. https://doi.org/10.1073/pnas.1604581113

Swenson, S., & Lawrence, D. (2014). Assessing a dry surface layer-based soil resistance parameterization for the community land model using GRACE and FLUXNET-MTE data. *Journal of Geophysical Research: Atmospheres*, *119*(17), 10299–10312. https://doi.org/10.1002/2014JD022314

Taylor, K. E., Stouffer, R. J., & Meehl, G. A. (2012). An overview of CMIP5 and the experiment design. *Bulletin of the American Meteorological Society*, *93*(4), 485–498. https://doi.org/10.1175/BAMS-D-11-00094.1

Thorne, J. H., Choe, H., Stine, P. A., Chambers, J. C., Holguin, A., Kerr, A. C., & Schwartz, M. W. (2018). Climate change vulnerability assessment of forests in the Southwest USA. *Climatic Change*, *148*(3), 387–402. https://doi.org/10.1007/s10584-017-2010-4

Trancoso, R., Larsen, J. R., McVicar, T. R., Phinn, S. R., & McAlpine, C. A. (2017). CO_2-vegetation feedbacks and other climate changes implicated in reducing base flow. *Geophysical Research Letters*, *44*(5), 2310–2318. https://doi.org/10.1002/2017GL072759

Ukkola, A., Keenan, T., Kelley, D. I., & Prentice, I. C. (2016). Vegetation plays an important role in mediating future water resources. *Environmental Research Letters*, *11*(9), 094022. https://doi.org/10.1088/1748-9326/11/9/094022

Viviroli, D., Dürr, H. H., Messerli, B., Meybeck, M., & Weingartner, R. (2007). Mountains of the world, water towers for humanity: Typology, mapping, and global significance. *Water Resources Research*, *43*(7), W07447. https://doi.org/10.1029/2006WR005653

Vose, R., Easterling, D. R., Kunkel, K., & Wehner, M. (2017). Temperature changes in the United States. In *Climate science special report: Fourth national climate assessment* (pp. 185–206). U.S. Global Change Research Program.

Xia, Y., Mitchell, K., Ek, M., Sheffield, J., Cosgrove, B., Wood, E., et al. (2012). Continental-scale water and energy flux analysis and validation for the North American land data assimilation system project phase 2 (NLDAS-2): 1. Intercomparison and application of model products. *Journal of Geophysical Research*, *117*(D3), D03109. https://doi.org/10.1029/2011JD016048

Xue, Y., Janjic, Z., Dudhia, J., Vasic, R., & De Sales, F. (2014). A review on regional dynamical downscaling in intraseasonal to seasonal simulation/prediction and major factors that affect downscaling ability. *Atmospheric Research*, *147*, 68–85. https://doi.org/10.1016/j.atmosres.2014.05.001

Yan, K., Park, T., Yan, G., Liu, Z., Yang, B., Chen, C., et al. (2016). Evaluation of MODIS LAI/FPAR product collection 6. Part 2: Validation and intercomparison. *Remote Sensing*, *8*(6), 460. https://doi.org/10.3390/rs8060460

Yang, Y., Donohue, R. J., McVicar, T. R., Roderick, M. L., & Beck, H. E. (2016). Long-term CO_2 fertilization increases vegetation productivity and has little effect on hydrological partitioning in tropical rainforests. *Journal of Geophysical Research: Biogeosciences*, *121*(8), 2125–2140. https://doi.org/10.1002/2016JG003475

Yang, Y., McVicar, T. R., Yang, D., Zhang, Y., Piao, S., Peng, S., & Beck, H. E. (2021). Low and contrasting impacts of vegetation CO_2 fertilization on global terrestrial runoff over 1982–2010: Accounting for aboveground and belowground vegetation–CO_2 effects. *Hydrology and Earth System Sciences*, *25*(6), 3411–3427. https://doi.org/10.5194/hess-25-3411-2021

Yang, Y., Roderick, M. L., Zhang, S., McVicar, T. R., & Donohue, R. J. (2019). Hydrologic implications of vegetation response to elevated CO_2 in climate projections. *Nature Climate Change*, *9*(1), 44–48. https://doi.org/10.1038/s41558-018-0361-0

Yang, Y., Zhang, S., Roderick, M. L., McVicar, T. R., Yang, D., Liu, W., & Li, X. (2020). Comparing Palmer drought severity index drought assessments using the traditional offline approach with direct climate model outputs. *Hydrology and Earth System Sciences*, *24*(6), 2921–2930. https://doi.org/10.5194/hess-24-2921-2020

Yang, Z. L., Niu, G. Y., Mitchell, K. E., Chen, F., Ek, M. B., Barlage, M., et al. (2011). The community Noah land surface model with multiparameterization options (Noah-MP): 2. Evaluation over global river basins. *Journal of Geophysical Research*, *116*(D12), D12110. https://doi.org/10.1029/2010JD015140

Yuan, H., Dai, Y., Xiao, Z., Ji, D., & Shangguan, W. (2011). Reprocessing the MODIS leaf area index products for land surface and climate modelling. *Remote Sensing of Environment*, *115*(5), 1171–1187. https://doi.org/10.1016/j.rse.2011.01.001

Zeng, X., Broxton, P., & Dawson, N. (2018). Snowpack change from 1982 to 2016 over conterminous United States. *Geophysical Research Letters*, *45*(23), 12940–12947. https://doi.org/10.1029/2018GL079621

Zeng, Z., Peng, L., & Piao, S. (2018). Response of terrestrial evapotranspiration to Earth's greening. *Current Opinion in Environmental Sustainability*, *33*, 9–25. https://doi.org/10.1016/j.cosust.2018.03.001

Zeng, Z., Piao, S., Li, L. Z., Zhou, L., Ciais, P., Wang, T., et al. (2017). Climate mitigation from vegetation biophysical feedbacks during the past three decades. *Nature Climate Change*, *7*(6), 432–436. https://doi.org/10.1038/nclimate3299

Zhang, X., Niu, G. Y., Elshall, A. S., Ye, M., Barron-Gafford, G. A., & Pavao-Zuckerman, M. (2014). Assessing five evolving microbial enzyme models against field measurements from a semiarid savannah—What are the mechanisms of soil respiration pulses? *Geophysical Research Letters*, *41*(18), 6428–6434. https://doi.org/10.1002/2014GL061399

Zhang, Y., Peña-Arancibia, J. L., McVicar, T. R., Chiew, F. H., Vaze, J., Liu, C., et al. (2016). Multi-decadal trends in global terrestrial evapotranspiration and its components. *Scientific Reports*, *6*(1), 1–12. https://doi.org/10.1038/srep19124

Zheng, H., Yang, Z. L., Lin, P., Wu, W. Y., Li, L., Xu, Z., et al. (2020). Falsification-oriented signature-based evaluation for guiding the development of land surface models and the enhancement of observations. *Journal of Advances in Modeling Earth Systems*, *12*(12), e2020MS002132. https://doi.org/10.1029/2020MS002132

Zhu, Q., Riley, W. J., Tang, J., Collier, N., Hoffman, F. M., Yang, X., & Bisht, G. (2019). Representing nitrogen, phosphorus, and carbon interactions in the E3SM land model: Development and global benchmarking. *Journal of Advances in Modeling Earth Systems*, *11*(7), 2238–2258. https://doi.org/10.1029/2018MS001571

Zhu, S., Chen, H., Zhang, X., Wei, N., Shangguan, W., Yuan, H., et al. (2017). Incorporating root hydraulic redistribution and compensatory water uptake in the Common Land Model: Effects on site level and global land modeling. *Journal of Geophysical Research: Atmospheres*, *122*(14), 7308–7322. https://doi.org/10.1002/2016JD025744

Zhu, Z., Piao, S., Lian, X., Myneni, R. B., Peng, S., & Yang, H. (2017). Attribution of seasonal leaf area index trends in the northern latitudes with "optimally" integrated ecosystem models. *Global Change Biology*, *23*(11), 4798–4813. https://doi.org/10.1111/gcb.13723